TABLE 1. Anti HIV-1 activity of novel SDP derivatives in PBMC[a]

Compound	IC_{50} value in p24 assay (nM)					
	HIV-1_{Ba-L} (R5)	HIV-1_{JRFL} (R5)	HIV-1_{MOKW} (R5)	HIV-1_{MM} ($R5_{MDR}$)	HIV-1_{JSL} ($R5_{MDR}$)	HIV-1_{NL4-3} (X4)
AK602	0.5 ± 0.3	0.2 ± 0.1	0.3 ± 0.2	0.7 ± 0.3	0.4 ± 0.2	>1,000
TAK779	14 ± 5	6 ± 2	9 ± 3	12 ± 4	10 ± 3	>1,000
SCH-C	3 ± 2	2 ± 1	2 ± 1.5	2.5 ± 1	2 ± 1	>1,000
ZDV	13 ± 5	7 ± 3	10 ± 6	520 ± 75	64 ± 13	9 ± 5
SQV	8 ± 3	6 ± 2	6 ± 3	212 ± 56	276 ± 44	10 ± 4

[a] IC_{50}s were determined by using PHA-PBMC isolated from three different donors, and the inhibition of p24 Gag protein production was used as an endpoint. All assays were conducted in triplicate. The results shown represent arithmetic means (±1 standard deviation) of three independently conducted assays. HIV-1_{MOKW} was isolated from a drug-naive AIDS patient, and HIV-1_{JSL} and HIV-1_{MM} were isolated from patients who received antiretroviral therapy for a long period of time and whose virus loads showed a number of RT and PR mutations. Two previously published CCR5 inhibitors, TAK779 and SCH-C, and zidovudine (ZDV) and saquinavar (SQV) were used as reference compounds.

45.1%]), resulting in the ratios of 1.43 and 1.40 (Fig. 5C and D), respectively. Figure 6A illustrates the overall profiles of $CD4^+/CD8^+$ cells ratios on day 16 in the four groups. The mean $CD4^+/CD8^+$ cell ratio in mice (n = 7) given saline was 0.1 (range, 0.06 to 0.20). In contrast, the ratios in AK602-treated mice (n = 8) were significantly higher with a mean value of 0.92 (range, 0.23 to 1.89; P = 0.001), which was comparable to that in ddI-treated mice (n = 9; mean, 1.29; range, 0.38 to 2.68; P = 0.001) and uninfected mice (n = 7; mean, 1.0; range, 0.50 to 1.49). The numbers of $CD4^+$ cells/μl

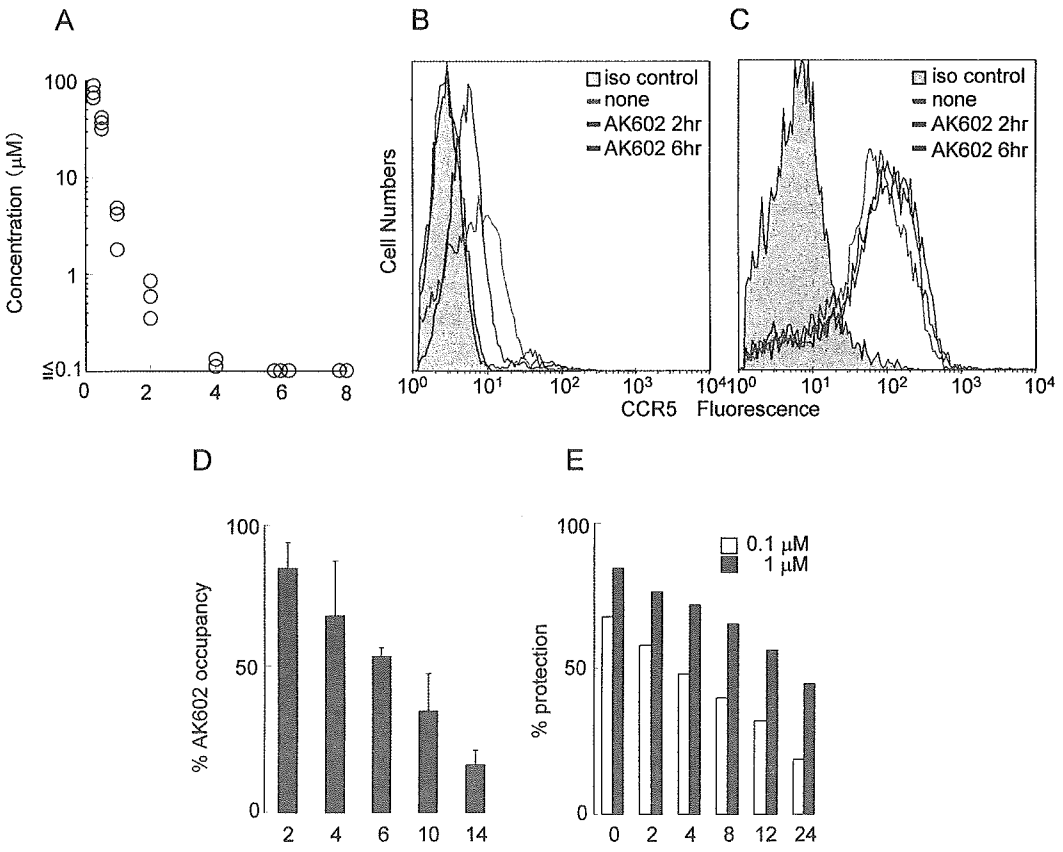

FIG. 4. Pharmacokinetics and persistence of anti-HIV-1 activity of AK602. (A) Pharmacokinetics of AK602. Each mouse was administered AK602 at a dose of 60 mg/kg, and blood samples were taken at 15, 30, 60, 120, 240, 480, and 720 min. Plasma concentrations of AK602 determined by HPLC analysis at 15, 30, 60, 120, and 240 min were 76.2, 36.1, 3.5, 0.6, and 0.13 μM, respectively. AK602 was not detected at later time points. (B and C) No CCR5 internalization or shedding was caused by AK602. Human PBMC were recovered 2 and 6 h after AK602 administration and stained with 45531 (B) or 3A9 (C). (D) Sustained AK602 occupancy on cell surfaces. At indicated periods of time after a bolus of AK-602 (60 mg/kg) was administered to hu-PBMC-NOG mice, PBMC were recovered and the percentages of AK602 occupancy on cellular CCR5 were determined with fluorescein isothiocyanate-conjugated monoclonal antibody 45531. (E) Persistence of in vitro activity of AK602 against R5 HIV-1 after AK602 depletion. $CCR5^+$ MAGI cells were exposed to 0.1 or 1 μM AK602 for 30 min and thoroughly washed to deplete AK602 from the medium. The cells were subsequently cultured for the indicated periods of time, exposed to HIV-1_{Ba-L}, and further cultured for 48 h, when the cells were harvested and lysed with Triton X-100-containing PBS. A solution containing chlorophenol red-β-D-galactopyranoside was added, the optical density was measured, and the percentage of protection was determined.

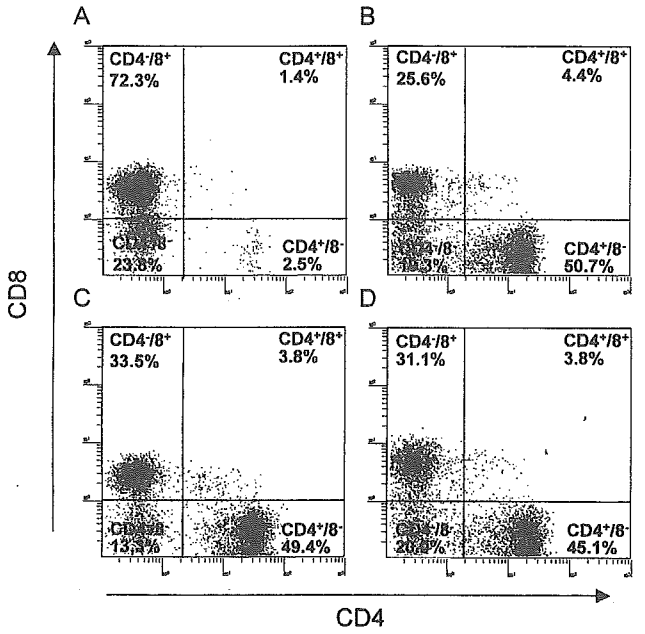

FIG. 5. Effects of AK602 on $CD4^+$ and $CD8^+$ cell counts in infected hu-PBMC-NOG mice. PBMC recovered on day 16 after R5 HIV-1 inoculation were subjected to flow cytometry. Shown are representative flow cytometric analysis profiles. Note that only 3.9% of $CD4^+$ cells were seen (A), resulting in a $CD4^+/CD8^+$ cell ratio of 0.05 in a mouse given saline, while distinct numbers of $CD4^+$ cells (55.1 and 53.2%) (B and C) were seen in AK602- and ddI-administered infected mice, resulting in $CD4^+/CD8^+$ cell ratios of 1.84 and 1.43, respectively. In an uninfected mouse (D), 48.9% of cells were positive for CD4, with a $CD4^+/CD8^+$ cell ratio of 1.40.

in saline-treated mice were significantly less than those of AK602-treated, ddI-treated, or uninfected mice (Fig. 6B).

Effects of AK602 on R5 HIV-1 proviral DNA copy numbers and serum p24 levels in R5 HIV-1-infected hu-PBMC-NOG mice. We next asked which population harbored proviral DNA in the cells recovered from R5 HIV-1-infected hu-PBMC-NOG mice, by purifying $CD4^+$ and $CD4^-$ cell populations and determining proviral DNA copy numbers in each population. As shown in Table 2, more than 99% of proviral DNA was found in $CD4^+$ cells and <0.3% of proviral DNA was detected in $CD4^-$ cells derived from saline-treated mice, indicating that R5 HIV-1 infection occurred in $CD4^+$ cells in the hu-PBMC-transplanted NOG environment. As illustrated in Fig. 6C, the mean number of R5 HIV-1 proviral DNA copies was 2.0×10^5 (range, 2.6×10^4 to 1.7×10^6) per 10^5 $CD4^+$ cells in R5 HIV-1-infected mice ($n = 7$) given saline. However, values for mice in groups given AK602 and ddI were 1.3×10^3 (range, 2.3×10^2 to 7.9×10^3; $P = 0.001$) and 1.8×10^2 (range, $<10^2$ to 7.9×10^2; $P = 0.001$), respectively.

The amounts of R5 HIV-1 p24 in serum were also found to be very high in saline-treated mice, with a mean amount of 1.1×10^5 pg/ml (range, 3.1×10^4 to 2.8×10^5 pg/ml). AK602 and ddI were found to significantly suppress the serum p24 amounts as examined on day 16 with a mean amount of 5.6×10^3 pg/ml (range, 8.1×10^2 to 2.1×10^4 pg/ml; $P = 0.001$) and 7.1×10^2 pg/ml (range, 1.3×10^2 to 1.1×10^4 pg/ml; $P = 0.001$), respectively (Fig. 6D).

AK602 suppressed R5 HIV-1 viremia in hu-PBMC-NOG mice. As described above, the PBMC transplanted to NOG mice were intensely activated in the xenogeneic environment and had undergone ~4 cycles of proliferation by day 2; a majority of the cells had undergone ≥10 cycles of proliferation by day 4 (Fig. 3B). These data suggested that R5 HIV-1 might extensively replicate in the hu-PBMC-NOG mice immediately after R5 HIV-1 inoculation. When we collected blood samples on days 5, 9, and 16 following the inoculation and determined R5 HIV-1 RNA copy numbers in infected, saline-treated mice ($n = 7$), the geometric mean copy number was 8.6×10^3/ml (range, 1.7×10^3 to 1.0×10^5) on day 5 and rapidly increased to 1.9×10^5/ml (range, 2.2×10^4 to 3.0×10^6) on day 9; by day 16, the mean copy number had reached 7.7×10^5/ml (range, 2.6×10^5 to 3.0×10^6/ml). However, AK602 significantly suppressed viremia by ~1.1 log, as examined on day 5; the mean numbers of R5 HIV-1 RNA copies in AK602-administered mice were 1.6 and 1.8 logs lower than those in saline-treated mice examined on days 9 and 16, respectively (Fig. 7). Comparable viremia suppression was seen in the mice receiving ddI (Fig. 7). It was noted that although AK602 did not completely prevent the viremia from further increasing after day 5, there was a clear reduction in the viremia increase rates. The mean slopes (change in RNA copies per day over the range of data from 5 to 16 days) for the group receiving saline was 0.167 ± 0.042, whereas those for the AK602 and ddI groups were 0.102 ± 0.041 and 0.091 ± 0.037, respectively. Thus, the rates of increase in the AK602 ($P = 0.0057$) and ddI ($P = 0.0023$) mice were significantly lower than that for the mice given saline, indicating that both of the agents significantly inhibited R5 HIV-1 replication in this mouse model over the range of days evaluated. No apparent AK602- or ddI-associated adverse effects were seen throughout the study period.

DISCUSSION

In the present hu-PBMC-NOG mouse model, human $CD4^+/CD8^+$ cell ratios went down to 0.1 by 16 days after R5 HIV-1 inoculation, the amounts of proviral DNA and p24 gag antigen reached 10^5 to 10^6 copies/10^5 $CD4^+$ cells and 10^5 pg/ml, respectively (Fig. 6), and no mice failed to be infected with R5 HIV-1. It is noteworthy that the use of NOG mice provides a higher engraftment rate than with other SCID mice such as NOD/Shi-SCID mice treated with anti-NK cell antibody or the β_2-microglobulin-deficient NOD-SCID mice (10). With NOG mice, the chimeric rate of 30 to 40% is achieved, and cord blood $CD34^+$ cells have been shown to "take" with as few as 100 cells (10). Moreover, all infected mice developed high levels of R5 HIV-1 viremia by day 16, reaching as high as 10^6 copies/ml (Fig. 7). It is worth noting that the notably high levels of HIV-1 viremia seen in the present mouse model by 16 days after R5 HIV-1 exposure can be seen only on acute infection or up to 10 years after HIV infection in humans (3, 4).

In the present study, we found that the conspicuous susceptibility to the infectivity and replication of R5 HIV-1 in these mice appeared to stem from the hyperactivation of the implanted human PBMC. The implanted PBMC were highly activated in the xenogeneic environment, expressed quite high

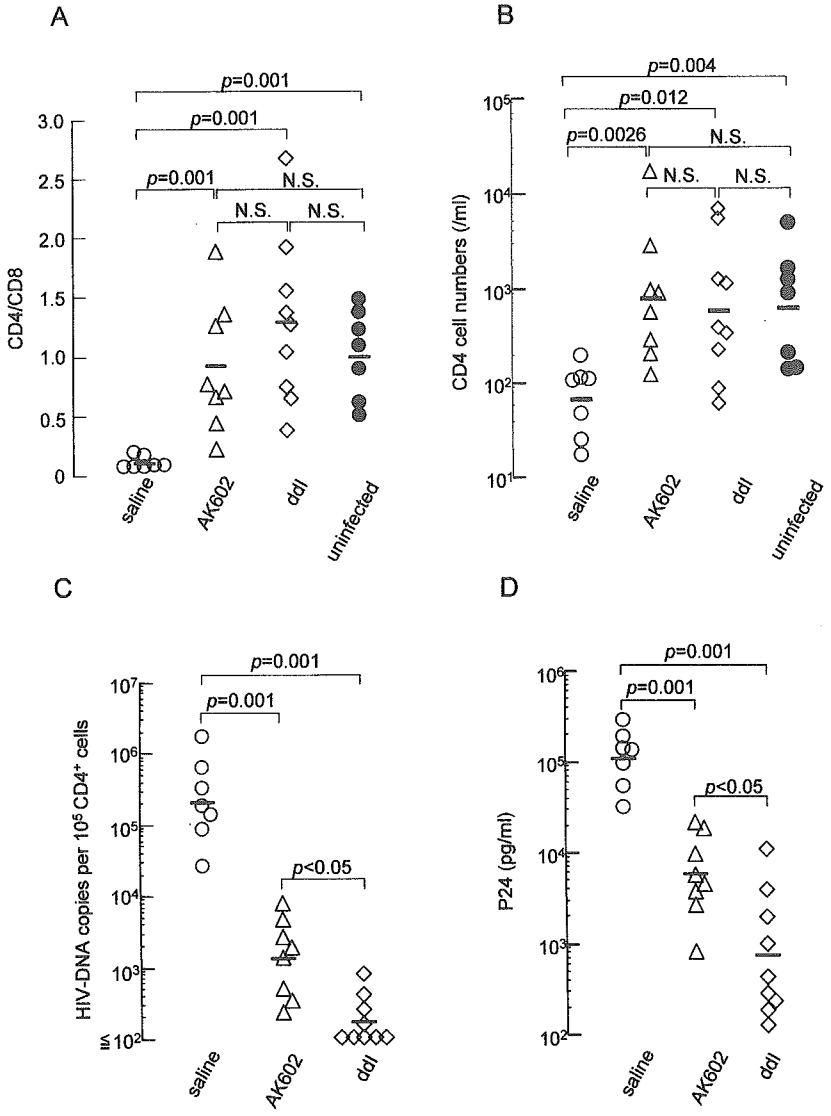

FIG. 6. Effects of AK602 on $CD4^+/CD8^+$ ratios and the amounts of proviral DNA and HIV-1 p24 in infected hu-PBMC-NOG mice. (A) Overall profiles of $CD4^+/CD8^+$ cell ratios. Note that the mean $CD4^+/CD8^+$ cell ratio in mice given saline ($n = 7$) was 0.1, while those in mice given AK602 or ddI were 0.92 and 1.29, respectively. The mean ratio in uninfected mice was 1.0. (B) Numbers of $CD4^+$ cells per microliter in each mouse group. (C) HIV-1 proviral DNA copy numbers in $CD4^+$ cells from each mouse group were determined by real-time PCR assay. Values are shown per 10^5 $CD4^+$ cells, as described in Materials and Methods. Note that the mean number of HIV-1 proviral DNA copies was 2.0×10^5 per 10^5 $CD4^+$ cells in mice given saline, while those in AK602- and ddI-treated groups were 1.3×10^3 and 1.8×10^2 per 10^5 $CD4^+$ cells (both, $P = 0.001$), respectively. (D) Amounts of plasma p24 antigen. Note that the amounts of p24 in plasma were high in saline-treated mice while AK602 and ddI significantly suppressed the serum p24 amounts as examined on day 16 after $HIV\text{-}1_{Ba\text{-}L}$ inoculation. The short bars indicate the arithmetic (A) and geometric (B, C, and D) means obtained.

levels of HLA-DR, and rapidly and continuously proliferated immediately after intraperitoneal infusion (Fig. 3A, B, and D). Moreover, the implanted PBMC expressed as much as 2.8-fold-higher levels of CCR5 on day 3 following implantation compared to PHA-PBMC on day 3 in culture (Fig. 3E). The combination of rapid proliferation and high levels of CCR5 expression of the implanted PBMC should explain the reason R5 HIV-1 rapidly replicated in the hu-PBMC-NOG mice and presented such high levels of R5 HIV-1 viremia. In this regard, only a few groups to date have documented the levels of viremia in the scientific literature. Among them are those by Garaci et al. (8) and Koyanagi et al. (14). The former documented high levels of viremia with a peak of 2.67×10^6 copies/ml in hu-PBL-NOD-SCID mice in which HIV-1-infected macrophages were inoculated, unlike our NOG mouse model where HIV-1 was directly inoculated. The latter report by Koyanagi et al. does not have viremia data but has data on p24 levels with a geometric mean of 11,092 pg/ml on day 14 after HIV-1 inoculation. However, the variation was much greater (178 to 1,434,444 pg/ml). Thus, one can say that the present model provides a greater reproducibility of high viremia levels than the mouse system reported by Koyanagi (14). It should be noted that the high levels of viremia and high engraftment rate achieved in this mouse model made it possible to monitor the

TABLE 2. Comparison of HIV-1 proviral DNA in human $CD4^+$ and $CD4^-$ cell fractions[a]

Sample	HIV-1 DNA copies (10^5 cells)		
	SCID-PBMC	$CD4^+$ cells	$CD4^-$ cells
Saline 1	138,858	162,193	461
Saline 2	135,967	117,949	<100
Saline 3	83,863	94,590	<100
AK602 1	3,390	2,300	<100
AK602 2	5,575	4,606	<100
AK602 3	1,925	1,398	<100
ddI 1	301	516	<100
ddI 2	793	1,317	<100
ddI 3	<100	118	<100

[a] HIV-1 proviral DNA copy numbers were determined by real-time PCR assay of unseparated human PBMC and purified $CD4^+$ and $CD4^-$ cells, following recovery from hu-PBMC-NOG mice. Values are shown per 10^5 cells, as described in Materials and Methods.

changes in the viremia levels periodically in the same set of mice without sacrificing them, while most of the previously described SCID mouse models required mice to be sacrificed at each time point of testing (25, 29, 30) or needed further in vitro coculture of the PBMC recovered from the mice with freshly prepared uninfected target cells for an additional period of days (9, 34).

We demonstrated in this study that a novel SDP derivative, AK602, exerted highly potent activity against laboratory and primary R5 HIV-1 strains as well as MDR R5 HIV-1 variant with IC_{50} values of subnanomolar concentrations (Table 1). It should be noted that AK602 represents a novel SDP derivative, which binds to human CCR5 but not to human CXCR4, CCR1, CCR2, CCR3, CCR4 or murine CCR5; blocks the binding of MIP-1α to CCR5 with an extremely high affinity (K_d values of ~3 nM); potently blocks HIV-1-gp120/CCR5 binding; and exerts potent activity against a wide spectrum of laboratory and primary R5 HIV-1 isolates including MDR HIV-1 and HIV-1 strains of various clades with IC_{50} values of 0.2 to 0.6 nM in vitro (K. Maeda, H. Ogata, S. Harada, Y. Tojo, T. Miyakawa, H. Nakata, Y. Takaoka, S. Shibayama, D. Fukushima, J. Moravek, E. Arnold, and H. Mitsuya, 11th Conf. Retrovir. Opp. Infect., abstr. 540, 2004; J. Demarest et al., XV Int. AIDS Conf., abstr. WeOrA1231, 2004). The plasma half-life of AK602 in the hu-PBMC-NOG mice, however, proved to be as short as 29 min when the agent was administered intraperitoneally (Fig. 4A). Considering that AK602 possesses such a high binding affinity to CCR5, we presumed that AK602 could remain on CCR5 for an extended period of time even after the agent was removed from the bloodstream in mice. The high and extensive level of AK602 occupancy observed in PBMC recovered from mice receiving AK602 substantiated this presumption (Fig. 4D). The subsequent in vitro experiment in which $CCR5^+$ MAGI cells were incubated with AK602 but exposed to R5 HIV-1 after the removal of the compound from the culture medium showed that AK602's anti-R5 HIV-1 activity can persist for an extensive period of time even if AK602 is no longer present in the culture (Fig. 4E). It is of note that unlike certain reports of in vivo anti-HIV-1 activity of chemokine antagonists which were administered before HIV-1 inoculation, thus demonstrating prophylactic effects of such agents (9, 30), the present system demonstrates anti-HIV-1 treatment after the establishment of HIV-1 infection, analogous to antiviral therapy in clinical settings.

When highly active antiretroviral therapy exerts its potent antiviral effects in clinical settings, a decrease in HIV-1 viremia is seen often within weeks, ultimately resulting in undetectable viremia; however in the present study, the viremia levels in mice receiving AK602 or ddI continued to increase although the rate of increment significantly declined (Fig. 7). The failure of AK602 and ddI to decrease viremia levels could be due in part to such a rapid viral replication in hyperactivated and proliferating $CD4^+$ cells. As discussed earlier, PBMC recovered from the hu-PBMC-NOG mice were highly positive for CCR5 and HLA-DR (Fig. 3D and E), compared to the levels of activation seen in the same donor's PHA-PBMC. It should be noted, however, that the mean numbers of proviral DNA copies on day 16 in mice receiving AK602 and ddI were 1.3×10^3 and 1.8×10^2 per 10^5 $CD4^+$ cells, respectively (Fig. 6C), suggesting that most $CD4^+$ cells (98.7 and 99.8% on average, respectively) were free of HIV-1 and proliferating in those

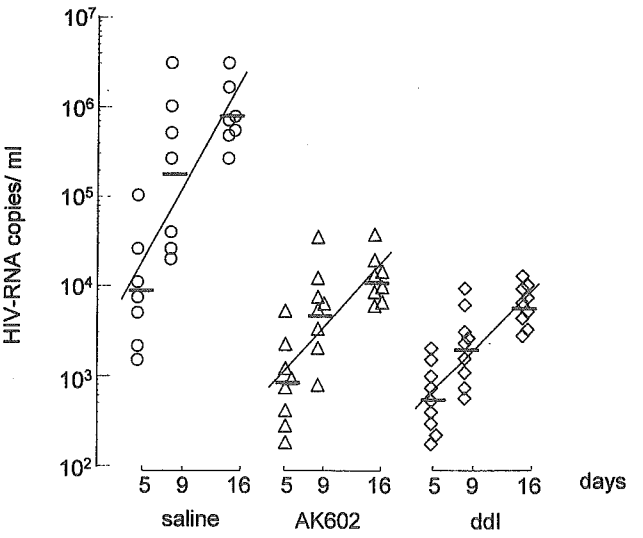

FIG. 7. AK602 suppresses R5 HIV-1 viremia in hu-PBMC-NOG mice. Blood samples were collected on days 5, 9, and 16 after inoculation and were subjected to the determination of R5 HIV-1 RNA copy numbers. Note that the copy numbers in saline-treated mice rapidly increased and reached ~10^6/ml by day 16, while AK602 significantly suppressed the viremia by 1.6 and 1.8 logs as examined on day 9 ($P = 0.001$ compared to saline-treated mice) and day 16 ($P = 0.001$), respectively. Comparable viremia suppression was seen in ddI-treated mice, except on day 16, when ddI activity was greater than that of AK602 ($P = 0.027$). Note that there was a clear reduction in the rate of increase of viremia as well. When the values of $\log_{10}$ HIV-1 RNA copies were calculated and the slopes corresponding to the rates of increase per day were determined, the resulting mean slope (solid line) for the saline-treated mice was 0.167 ± 0.042, whereas those for the AK602- and ddI-treated mice were 0.102 ± 0.041 and 0.091 ± 0.037, respectively. The increase rate for saline-treated mice was significantly higher than those of AK602-treated mice ($P = 0.0057$) and ddI-treated mice ($P = 0.0023$), respectively. The horizontal bars and solid lines represent the geometric means of HIV-1 RNA copy numbers and the slopes calculated, respectively.

mice on day 16 after the virus inoculation, if one copy of proviral DNA was postulated to reside in one $CD4^+$ cell.

One of us (Y.K.) previously attempted to investigate the mechanism of $CD4^+$ cell depletion seen in individuals with HIV-1 infection by employing a PBMC-transplanted NOD (NOD/Shi) *scid/scid* mouse system (24). Massive apoptosis was observed in HIV-1-uninfected $CD4^+$ cells in the spleens of the HIV-1-infected NOD-*scid/scid* mice. A combination of terminal deoxynucleotidyl transferase-mediated dUTP nick-end labeling and immunostaining for death-inducing tumor necrosis factor (TNF) family molecules showed that apoptotic cells were frequently found in conjugation with TNF-related apoptosis-inducing ligand (TRAIL)-expressing $CD3^+$ $CD4^+$ human T cells. Further observation that a neutralizing anti-TRAIL antibody inhibited the development of $CD4^+$ cell apoptosis suggested that a large number of HIV-1-uninfected $CD4^+$ cells undergo TRAIL-mediated apoptosis, contributing to the marked depletion of $CD4^+$ cells (24). The observation by Miura and his colleagues that the number of TRAIL-positive cells was consistently higher in HIV-1-infected mice than in uninfected ones makes it apparent that TRAIL expression is induced upon HIV-1 infection (23, 24). In this regard, the present observation that AK602 and ddI potently blocked the decrease in $CD4^+$ cells in spite of the rather increasing HIV-1 viremia in the face of AK602 or ddI (Fig. 7) suggests that the mere presence of viremia might not be sufficient for the HIV-induced apoptosis in $CD4^+$ cells. Our observation that most surviving $CD4^+$ cells in mice receiving AK602 or ddI were free of HIV-1 (see above) suggests that these anti-HIV-1 agents might block not only de novo HIV-1 infection, but also bystander killing of uninfected $CD4^+$ cells. The present data also suggest that a certain factor(s) such as cytokines produced by the freshly HIV-1-infected cells might mediate the apoptosis of bystander $CD4^+$ cells through the upregulation of TRAIL expression, death receptors (e.g., DR4 and DR5), and/or downregulation of decoy receptors (e.g., DcR1 and DcR2) (26, 27). However, experiments with a combination of terminal deoxynucleotidyl transferase-mediated dUTP nick-end labeling and TNF family molecules have to be conducted for better understanding of the bystander killing in regard to AK602's effects.

It is of note that several CCR5 antagonists are currently in various stages of development. AK602 has recently been administered to healthy adult subjects in a phase I clinical trial and shown to bind to CCR5 for an extended period of time, suggesting that an oral formulation with fewer administrations and lower dosage is possible for AK602 as a therapeutic agent for HIV-1 infection (J. Demarest, K. Adkison, S. Sparks, A. Shachoy-Clark, K. Schell, S. Reddy, L. Fang, K. O'Mara, S. Shibayama, and S. Piscitelli, 11th Conf. Retrovir. Opp. Infect., abstr. 139, 2004). Taken together, our observations that plasma viral load reached $\sim 10^6$ RNA copies/ml and that AK602 potently inhibited the replication of R5 HIV-1 strongly suggest that the present hu-PBMC-NOG mouse AIDS model could serve as a useful instrument for analyzing the pathogenesis of HIV-1 infection and testing the efficacy of antiviral agents.

ACKNOWLEDGMENTS

We thank Seth Steinberg for statistical analysis and Naoko Misawa, Yuji Kawano, and Hiromi Ogata for technical assistance and discussion.

This work was supported in part by grant-in-aids for Scientific Research on Priority Areas (14207025 and 15019086) from the Japanese Ministry of Education, Science, Sports, Culture and Technology of Japan (Monbu-Kagakusho) and a grant for AIDS Research (H15-AIDS-001) from the Ministry of Health, Labor, and Welfare of Japan (Kosei-Rohdosho).

REFERENCES

1. **Baba, M., O. Nishimura, N. Kanzaki, M. Okamoto, H. Sawada, Y. Iizawa, M. Shiraishi, Y. Aramaki, K. Okonogi, Y. Ogawa, K. Meguro, and M. Fujino.** 1999. A small-molecule, nonpeptide CCR5 antagonist with highly potent and selective anti HIV-1 activity. Proc. Natl. Acad. Sci. USA **96:**5698–5703.
2. **Carr, A., K. Samaras, A. Thorisdottir, G. R. Kaufmann, D. J. Chisholm, and D. A. Cooper.** 1999. Diagnosis, prediction, and natural course of HIV-1 protease-inhibitor associated lipodystrophy, hyperlipidaemia, and diabetes mellitus: a cohort study. Lancet **353:**2093–2099.
3. **Dean, M., M. Carrington, C. Winkler, G. A. Huttley, M. W. Smith, R. Allikmets, J. J. Goedert, S. P. Buchbinder, E. Vittinghoff, E. Gomperts, S. Donfield, D. Vlahov, R. Kaslow, A. Saah, C. Rinaldo, R. Detels, and S. J. O'Brien.** 1996. Genetic restriction of HIV-1 infection and progression to AIDS by a deletion allele of the CKR5 structural gene. Hemophilia Growth and Development Study, Multicenter AIDS Cohort Study, Multicenter Hemophilia Cohort Study, San Francisco City Cohort, ALIVE Study. Science **273:**1856–1862.
4. **Easterbrook, P. J.** 1999. Long-term non-progression in HIV infection: definitions and epidemiological issues. J. Infect. **38:**71–73.
5. **Fauci, A. S.** 1999. The AIDS epidemic—considerations for the 21st century. N. Engl. J. Med. **341:**1046–1050.
6. **Finzi, D., J. Blankson, J. D. Siliciano, J. B. Margolick, K. Chadwick, T. Pierson, K. Smith, J. Lisziewicz, F. Lori, C. Flexner, T. C. Quinn, R. E. Chaisson, E. Rosenberg, B. Walker, S. Gange, J. Gallant, and R. F. Siliciano.** 1999. Latent infection of CD4+ T cells provides a mechanism for lifelong persistence of HIV-1, even in patients on effective combination therapy. Nat. Med. **5:**512–517.
7. **Gartner, S., P. Markovits, D. M. Markovitz, M. H. Kaplan, R. C. Gallo, and M. Popovic.** 1986. The role of mononuclear phagocytes in HTLV-III/LAV infection. Science **233:**215–219.
8. **Garaci, E., S. Aquaro, C. Lapenta, A. Amendola, M. Spada, S. Covaceuszach, C. F. Perno, and F. Belardelli.** 2003. Anti-nerve growth factor Ab abrogates macrophage-mediated HIV-1 infection and depletion of CD4+ T lymphocytes in hu-SCID mice. Proc. Natl. Acad. Sci. USA **100:**8927–8932.
9. **Ichiyama, K., S. Yokoyama-Kumakura, Y. Tanaka, R. Tanaka, K. Hirose, K. Bannai, T. Edamatsu, M. Yanaka, Y. Niitani, N. Miyano-Kurosaki, H. Takaku, Y. Koyanagi, and N. Yamamoto.** 2003. A duodenally absorbable CXC chemokine receptor 4 antagonist, KRH-1636, exhibits a potent and selective anti-HIV-1 activity. Proc. Natl. Acad. Sci. USA **100:**4185–4190.
10. **Ito, M., H. Hiramatsu, K. Kobayashi, K. Suzue, M. Kawahata, K. Hioki, Y. Ueyama, Y. Koyanagi, K. Sugamura, K. Tsuji, T. Heike, and T. Nakahata.** 2002. NOD/SCID/γ(c)(null) mouse: an excellent recipient mouse model for engraftment of human cells. Blood **100:**3175–3182.
11. **Kavlick, M. F., and H. Mitsuya.** 2001. The emergence of drug resistant HIV-1 variants and its impact on antiretroviral therapy of HIV-1 infection, p. 279–312. *In* E. De Clercq (ed.), The art of antiretroviral therapy. American Society for Microbiology, Washington, D.C.
12. **Koh, Y., H. Nakata, K. Maeda, H. Ogata, G. Bilcer, T. Devasamudram, J. F. Kincaid, P. Boross, Y. F. Wang, Y. Tie, P. Volarath, L. Gaddis, R. W. Harrison, I. T. Weber, A. K. Ghosh, and H. Mitsuya.** 2003. Novel bis-tetrahydrofuranylurethane-containing nonpeptidic protease inhibitor (PI) UIC-94017 (TMC114) with potent activity against multi-PI-resistant human immunodeficiency virus in vitro. Antimicrob. Agents Chemother. **47:**3123–3129.
13. **Koyanagi, Y., S. Miles, R. T. Mitsuyasu, J. E. Merrill, H. V. Vinters, and I. S. Chen.** 1987. Dual infection of the central nervous system by AIDS viruses with distinct cellular tropisms. Science **236:**819–822.
14. **Koyanagi, Y., Y. Tanaka, J. Kira, M. Ito, K. Hioki, N. Misawa, Y. Kawano, K. Yamasaki, R. Tanaka, Y. Suzuki, Y. Ueyama, E. Terada, T. Tanaka, M. Miyasaka, T. Kobayashi, Y. Kumazawa, and N. Yamamoto.** 1997. Primary human immunodeficiency virus type 1 viremia and central nervous system invasion in a novel hu-PBL-immunodeficient mouse strain. J. Virol. **71:**2417–2424.
15. **Lee, B., M. Sharron, L. J. Montaner, D. Weissman, and R. W. Doms.** 1999. Quantification of CD4, CCR5, and CXCR4 levels on lymphocyte subsets, dendritic cells, and differentially conditioned monocyte-derived macrophages. Proc. Natl. Acad. Sci. USA **96:**5215–5220.
16. **Lyons, A. B.** 2000. Analysing cell division in vivo and in vitro using flow cytometric measurement of CFSE dye dilution. J. Immunol. Methods **243:**147–154.
17. **Maeda, K., K. Yoshimura, S. Shibayama, H. Habashita, H. Tada, K. Sagawa, T. Miyakawa, M. Aoki, D. Fukushima, and H. Mitsuya.** 2001. Novel low molecular weight spirodiketopiperazine derivatives potently inhibit R5

HIV-1 infection through their antagonistic effects on CCR5. J. Biol. Chem. **276**:35194–35200.
18. **Maeda, Y., M. Foda, S. Matsushita, and S. Harada.** 2000. Involvement of both the V2 and V3 regions of the CCR5-tropic human immunodeficiency virus type 1 envelope in reduced sensitivity to macrophage inflammatory protein 1α. J. Virol. **74**:1787–1793.
19. **McCune, J. M., R. Namikawa, C. C. Shih, L. Rabin, and H. Kaneshima.** 1990. Suppression of HIV infection in AZT-treated SCID-hu mice. Science **247**:564–566.
20. **Mitsuya, H., and S. Broder.** 1986. Inhibition of the in vitro infectivity and cytopathic effect of human T-lymphotropic virus type III/lymphadenopathy virus-associated virus (HTLV-III/LAV) by 2′,3′-dideoxynucleosides. Proc. Natl. Acad. Sci. USA **83**:1911–1915.
21. **Mitsuya, H., and S. Broder.** 1987. Strategies for antiviral therapy in AIDS. Nature **325**:773–778.
22. **Mitsuya, H., and J. Erickson.** 1999. Discovery and development of antiretroviral therapeutics for HIV infection, p. 751–780. *In* T. C. Merigan, J. G. Bartlet, and D. Bolognesi (ed.), Textbook of AIDS medicine. Williams & Wilkins, Baltimore, Md.
23. **Miura, Y., N. Misawa, Y. Kawano, H. Okada, Y. Inagaki, N. Yamamoto, M. Ito, H. Yagita, K. Okumura, H. Mizusawa, and Y. Koyanagi.** 2003. Tumor necrosis factor-related apoptosis-inducing ligand induces neuronal death in a murine model of HIV central nervous system infection. Proc. Natl. Acad. Sci. USA **100**:2777–2782.
24. **Miura, Y., N. Misawa, N. Maeda, Y. Inagaki, Y. Tanaka, M. Ito, N. Kayagaki, N. Yamamoto, H. Yagita, H. Mizusawa, and Y. Koyanagi.** 2001. Critical contribution of tumor necrosis factor-related apoptosis-inducing ligand (TRAIL) to apoptosis of human CD4+ T cells in HIV-1-infected hu-PBL-NOD-SCID mice. J. Exp. Med. **193**:651–660.
25. **Mosier, D. E., R. J. Gulizia, S. M. Baird, D. B. Wilson, D. H. Spector, and S. A. Spector.** 1991. Human immunodeficiency virus infection of human-PBL-SCID mice. Science **251**:791–794.
26. **Pan, G., J. Ni, Y. F. Wei, G. Yu, R. Gentz, and V. M. Dixit.** 1997. An antagonist decoy receptor and a death domain-containing receptor for TRAIL. Science **277**:815–818.
27. **Pan, G., K. O'Rourke, A. M. Chinnaiyan, R. Gentz, R. Ebner, J. Ni, and V. M. Dixit.** 1997. The receptor for the cytotoxic ligand TRAIL. Science **276**:111–113.
28. **Ratain, M., and W. Plunkett.** 1997. Pharmacology, p. 875–889. *In* J. Holland, R. Bast, Jr., D. Morton, E. Frei, D. KuFe, and R. Weichselbaum (ed.), Cancer medicine, 4th ed. Williams and Wilkins, Baltimore, Md.
29. **Ruxrungtham, K., E. Boone, H. Ford, Jr., J. S. Driscoll, R. T. Davey, Jr., and H. C. Lane.** 1996. Potent activity of 2′-β-fluoro-2′,3′-dideoxyadenosine against human immunodeficiency virus type 1 infection in hu-PBL-SCID mice. Antimicrob. Agents Chemother. **40**:2369–2374.
30. **Strizki, J. M., S. Xu, N. E. Wagner, L. Wojcik, J. Liu, Y. Hou, M. Endres, A. Palani, S. Shapiro, J. W. Clader, W. J. Greenlee, J. R. Tagat, S. McCombie, K. Cox, A. B. Fawzi, C. C. Chou, C. Pugliese-Sivo, L. Davies, M. E. Moreno, D. D. Ho, A. Trkola, C. A. Stoddart, J. P. Moore, G. R. Reyes, and B. M. Baroudy.** 2001. SCH-C (SCH 351125), an orally bioavailable, small molecule antagonist of the chemokine receptor CCR5, is a potent inhibitor of HIV-1 infection in vitro and in vivo. Proc. Natl. Acad. Sci. USA **98**:12718–12723.
31. **Walker, U. A., B. Setzer, and N. Venhoff.** 2002. Increased long-term mitochondrial toxicity in combinations of nucleoside analogue reverse-transcriptase inhibitors. AIDS **16**:2165–2173.
32. **Westervelt, P., H. E. Gendelman, and L. Ratner.** 1991. Identification of a determinant within the human immunodeficiency virus 1 surface envelope glycoprotein critical for productive infection of primary monocytes. Proc. Natl. Acad. Sci. USA **88**:3097–3101.
33. **Yahata, T., K. Ando, Y. Nakamura, Y. Ueyama, K. Shimamura, N. Tamaoki, S. Kato, and T. Hotta.** 2002. Functional human T lymphocyte development from cord blood CD34+ cells in nonobese diabetic/Shi-scid, IL-2 receptor gamma null mice. J. Immunol. **169**:204–209.
34. **Yoshida, A., R. Tanaka, T. Murakami, Y. Takahashi, Y. Koyanagi, M. Nakamura, M. Ito, N. Yamamoto, and Y. Tanaka.** 2003. Induction of protective immune responses against R5 human immunodeficiency virus type 1 (HIV-1) infection in hu-PBL-SCID mice by intrasplenic immunization with HIV-1-pulsed dendritic cells: possible involvement of a novel factor of human CD4(+) T-cell origin. J. Virol. **77**:8719–8728.
35. **Yoshimura, K., R. Kato, K. Yusa, M. F. Kavlick, V. Maroun, A. Nguyen, T. Mimoto, T. Ueno, M. Shintani, J. Falloon, H. Masur, H. Hayashi, J. Erickson, and H. Mitsuya.** 1999. JE-2147: a dipeptide protease inhibitor (PI) that potently inhibits multi-PI-resistant HIV-1. Proc. Natl. Acad. Sci. USA **96**: 8675–8680.

Structure-Based Design: Synthesis and Biological Evaluation of a Series of Novel Cycloamide-Derived HIV-1 Protease Inhibitors

Arun K. Ghosh,*,† Lisa M. Swanson,† Hanna Cho,† Sofiya Leshchenko,† Khaja Azhar Hussain,† Stephanie Kay,† D. Eric Walters,‡ Yasuhiro Koh,§ and Hiroaki Mitsuya§,||

Department of Chemistry, University of Illinois at Chicago, 845 West Taylor Street, Chicago, Illinois 60607, Department of Biological Chemistry, Rosalind Franklin University of Medicine and Science, North Chicago, Illinois 60064, Department of Hematology and Infectious Diseases, Kumamoto University School of Medicine, Kumamoto 860-8556, Japan, and Experimental Retrovirology Section, HIV and AIDS Malignancy Branch, National Cancer Institute, Bethesda, Maryland 20892

Received January 8, 2005

The structure-based design and synthesis of a series of novel nonpeptide HIV protease inhibitors are described. The inhibitors were designed based upon the X-ray crystal structure of inhibitor **1** (UIC-94017)-bound HIV-1 protease. The inhibitors incorporated 3-hydroxysalicyclic acid-derived acyclic and cyclic P2 ligand into the (*R*)-(hydroxyethylamino)sulfonamide isostere. The inhibitors contain only two chiral centers and are readily synthesized in optically active form utilizing Sharpless asymmetric epoxidation, regioselective epoxide opening, and ring-closing olefin metathesis using Grubbs' catalyst as the key steps. We have synthesized 13−15-membered cycloamides and evaluated their HIV-1 protease enzyme inhibitory and antiviral activities in MT-2 cells. Interestingly, all cycloamide-derived inhibitors are noticeably more potent than the corresponding acyclic compounds. The ring size and substituent effects were investigated. It turned out that the 14-membered saturated ring is preferred by the S_1-S_2 active sites of HIV-1 protease. Macrocycle **26** showed excellent enzyme inhibitory potency with a K_i value of 0.7 nM and an antiviral IC_{50} value of 0.3 μM. In view of their structural simplicity and preliminary interesting results, further optimization of these inhibitors is underway.

Introduction

The global pandemic of HIV/AIDS is one of the most extraordinary humanitarian and medical challenges of our time. Combination therapy or highly active antiretroviral therapy with HIV protease inhibitors and reverse transcriptase inhibitors has become the major current treatment regimen for AIDS.[1] Our recent structure-based designed strategies enhancing backbone binding led to the discovery of a nonpeptidyl HIV protease inhibitor **1** (UIC-94017, now renamed as TMC-114; Figure 1), which is exceedingly potent against wild-type (K_i = 15 ± 1 pM, n = 4 and ID_{50} = 1.4 ± 0.25 nM, n = 5) and resistant viruses.[2,3] It is currently undergoing advanced clinical trials.[4] In inhibitor **1**, we incorporated a structure-based designed bis-tetrahydrofuran as the P_2 ligand in (*R*)-(hydroxyethylamino)sulfonamide isostere.[5] A high-resolution X-ray crystal structure of this inhibitor-bound HIV-1 protease structure revealed critical ligand-binding site interaction in the HIV protease active site.[6] Upon the basis of this structure, we subsequently speculated that various 13−15-membered macrocycles involving P_1-P_2 ligands would effectively hydrogen bond with the critical Asp-29 and Asp-30 backbone residues and tight-bound water molecule as well as fill in the hydrophobic pockets of S_1-S_2 binding sites. In an effort to introduce structural diversity, we have designed and explored 2,3-dihydroxybenzoic acid-derived 13−15-membered cycloamides as P_1-P_2 ligands, which could conceivably make critical interactions in the S_1-S_2 binding sites. Herein, we report our preliminary results of these investigations. The inhibitors were synthesized stereoselectively by using Sharpless asymmetric epoxidation and subsequent regioselective opening of epoxide rings as the key steps. Cycloamide

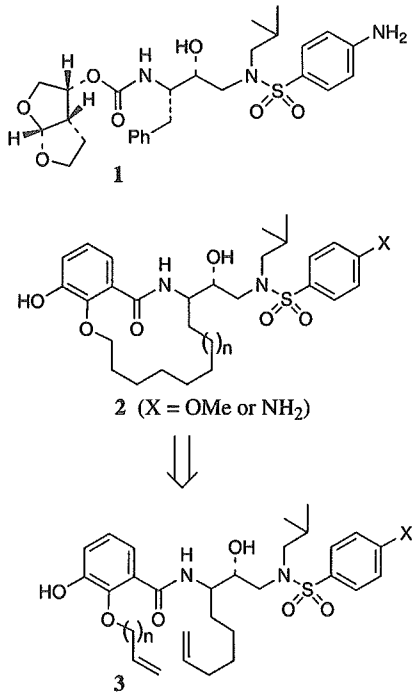

Figure 1. Structures of inhibitors **1** and cyclic and acyclic inhibitors.

* To whom correspondence should be addressed. Tel: 312-996-9672. Fax: 312-996-1547. E-mail: arunghos@uic.edu.
† University of Illinois at Chicago.
‡ Rosalind Franklin University of Medicine and Science.
§ Kumamoto University School of Medicine.
|| National Cancer Institute.

10.1021/jm050019i CCC: $30.25
Published on Web 04/15/2005

Scheme 1[a]

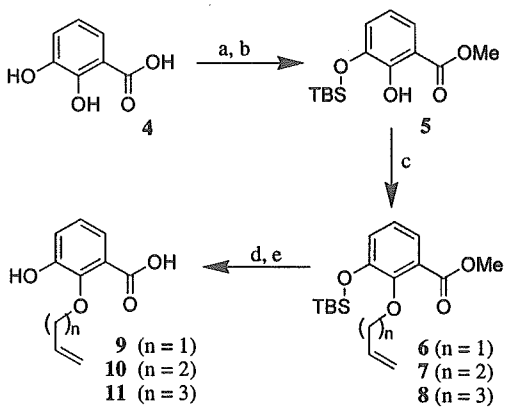

[a] Reagents and conditions: (a) Cs_2CO_3, MeOH–H_2O, 23 °C; then MeI, DMF, 0–23 °C. (b) TBSCl, *i*-Pr_2NEt, DMF, 0 °C. (c) Allylic alcohol, DEAD, PPh_3, THF, 23 °C. (d) TBAF, THF, 0 °C. (e) LiOH, THF, H_2O, 55 °C.

Scheme 2[a]

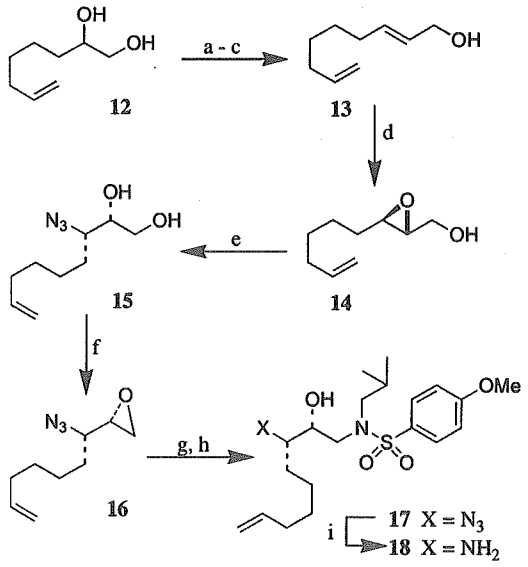

[a] Reagents and conditions: (a) $NaIO_4$, THF, H_2O, 23 °C. (b) $(EtO)_2P(O)CH_2CO_2Et$, NaH, THF, 0–23 °C. (c) DIBAL-H, CH_2Cl_2, −78 °C. (d) (−)-DET, 4 Å MS, Ti(*i*-OPr)$_4$, TBHP, CH_2Cl_2, −20 °C. (e) Ti(*i*-OPr)$_4$, $TMSN_3$, benzene, 90 °C. (f) $AcOCMe_2COCl$, $CHCl_3$, 0 °C; then NaOMe, THF, 23 °C. (g) $(CH_3)_2CHCH_2NH_2$, *i*-PrOH, 90 °C. (h) 4-MeO-Ph-SO_2Cl, 1:1 (CH_2Cl_2, aqueous $NaHCO_3$), 23 °C. (i) $LiAlH_4$, THF, 23 °C.

derivatives were prepared efficiently by using ring-closing olefin metathesis.

Chemistry

The synthesis of 3-hydroxysalicyclic acid-based non-peptidyl P_2 ligands is illustrated in Scheme 1. Esterification of commercially available 3-hydroxysalicyclic acid with Cs_2CO_3 in MeOH followed by selective protection of the 3-hydroxyl group as the TBS ether provided **5** in 78% yield. Ester **5** was then converted to allyl ethers and its homologues (**6**–**8**) using Mitsunobu conditions[7] in 58–89% yields. Removal of the TBS ether followed by saponification of the ester afforded various acids **9**–**11** in 83–94% yields.

Enantioselective synthesis of requisite hydroxyethylamine sulfonamide isostere is outlined in Scheme 2. Commercially available diol **12** was converetd to allylic alcohol **13** in a three-step sequence involving (i) oxidative cleavage of diol **12** with $NaIO_4$; (ii) Horner–Emmons olefination of the resulting aldehyde to α,β-unsaturated ester; and (iii) DIBAL-H reduction of ester to alcohol **13**. The allylic alcohol **13** was subjected to the Sharpless asymmetric epoxidation[8] condition with (−)-diethyl-D-tartrate to furnish the epoxide **14** in 78% yield. Regioselective ring opening of epoxide **14** with diisopropoxytitanium diazide in benzene at 90 °C, as described by Sharpless and co-workers,[9] provided the azidodiol **15** in near quantitative yield. The diol was converted to the azidoepoxide **16** by treatment with 2-acetoxyisobutyryl chloride in chloroform at 23 °C followed by exposure of the resulting chloro acetate derivative to NaOMe to afford **16**.[10] Sulfonamide **17** was synthesized in a two-step sequence by first opening the epoxide with isobutylamine and subsequent reaction of the amine with *para*-methoxybenzenesulfonyl chloride to afford sulfonamide **17** in 58% yield. Reduction of the azides by $LiAlH_4$ furnished the amine **18**, which was used directly for the next reaction without further purification.

Scheme 3[a]

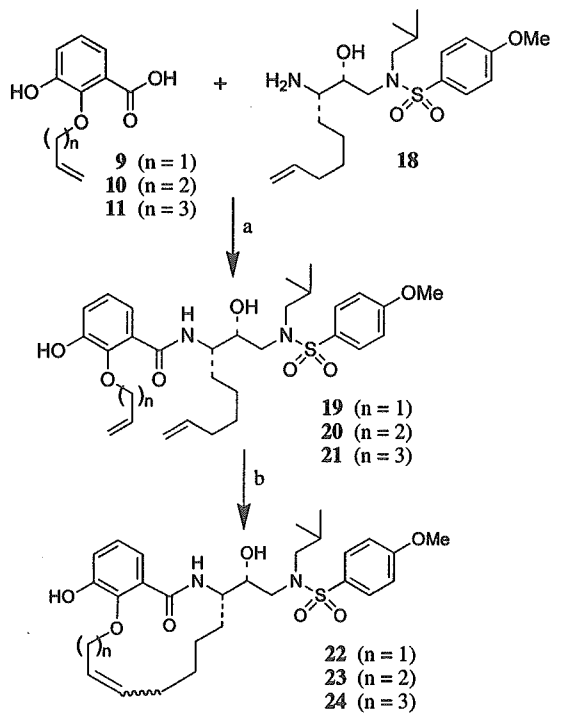

[a] Reagents and conditions: (a) EDC, HOBt, Et_3N, DMF, 0–23 °C. (b) Grubbs' cat. (first generation), CH_2Cl_2, 23 °C.

Synthesis of various acyclic inhibitors and subsequent preparation of cyclic derivatives is carried out according to Scheme 3. Using a standard peptide coupling procedure,[11] amine **18** was reacted with carboxylic acids **9**–**11** in the presence of N-ethyl-N′-(dimethylaminopropyl)-carbodiimide hydrochloride (EDC), triethylamine, and 1-hydroxybenzotriazole hydrate (HOBt) in DMF to furnish various acyclic inhibitors **19**–**21** in 50–76% yields. Ring-closing olefin metathesis of these acyclic derivatives with commercial first generation Grubbs' catalyst[12] (10 mol %) in CH_2Cl_2 (0.003 M solution) afforded 13–15-membered unsaturated cycloamides **22**–**24** in excellent yield (89–96%).

As shown in Scheme 4, catalytic hydrogenation of 13-membered unsatuarated inhibitor **22** in the presence

Scheme 4[a]

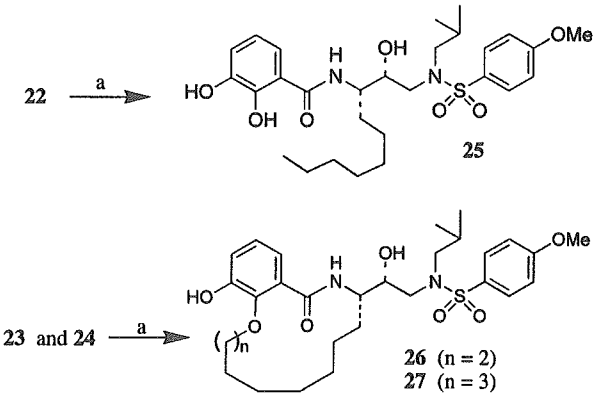

[a] Reagents and conditions: (a) H_2, 10% Pd–C, MeOH, 23 °C.

of 10% Pd–C did not provide the corresponding saturated cycloamides. Instead, hydrogenation resulted in cleavage of the phenolic ether to give phenol **25** in 63% yield. Bergmann and Heimhold[13] have previously reported similar cleavage of allylic ethers of phenol during hydrogenation reaction. Attempts to reduce the allylic double bond of **22** under different hydrogenation conditions (Lindlar catalyst, 5% Pd on $BaSO_4$, Rh on alumina, and Wilkinson's catalyst) failed to give the desired product, resulting in either the cleaved ether or the recovery of starting material. Besides hydrogenation, reduction with $NaBH_4$ and $CoCl_2$[14] also resulted in the ether cleavage. Catalytic hydrogenation of the unsaturated cycloamides **23** and **24**, however, furnished the saturated macrocycles **26** and **27** in good yields (69–78%).

The synthesis of saturated 13-membered cycloamide was then carried out by an alternative route. Amino alcohol **28** was prepared enantioselectively following the route outlined in Scheme 2 from 5-hexenal, which was obtained by PCC oxidation of commercial 5-hexene-1-ol. Coupling of carboxylic acid **10** and amine **28** in the presence of EDC, HOBt, and Et_3N in DMF afforded the amide derivative **29**. It was converted to saturated 13-membered cycloamide derivative **30** in a two-step sequence by exposure of **29** to commercial first generation Grubbs' catalyst[12] (10 mol %) in CH_2Cl_2 followed by catalytic hydrogenation of the resulting unsaturated cycloamide in the presence of 10% Pd–C in methanol to provide **30** in 71% yield for two steps.

The synthesis of 14-membered inhibitor **33** was carried out as described in Scheme 6. Opening of epoxide **16** with isobutylamine and reaction of the resulting amine with 3,4-methylenedioxybenzene sulfonyl chloride[15] followed by LAH reduction of the azide afforded the amine **31** in 61% yield. It was coupled with acid **10** under standard reaction conditions to furnish the acyclic inhibitor **32** in 57% yield. Exposure of **32** to Grubbs' catalyst[12] under dilute conditions (0.002 M CH_2Cl_2) afforded the corresponding unsaturated macrocycle, which upon hydrogenation furnished the saturated inhibitor **33** in 82% yield for two steps.

Biological Evaluation and Discussion

The inhibitory potencies of various acyclic and cyclic inhibitors in Table 1 were measured by the assay protocol of Toth and Marshall.[17] The values with standard deviation denote the mean values from three

Scheme 5[a]

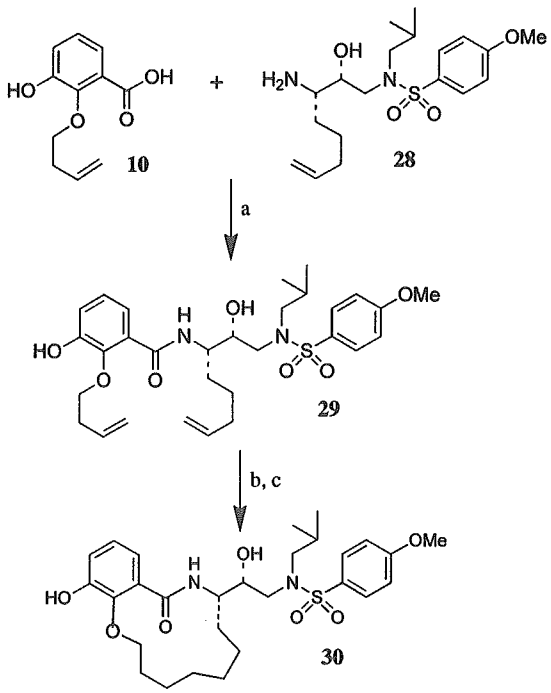

[a] Reagents and conditions: (a) EDC, HOBt, Et_3N, DMF, 0–23 °C. (b) Grubbs' cat. (first generation), CH_2Cl_2, 23 °C. (c) H_2, 10% Pd–C, MeOH, 23 °C.

Scheme 6[a]

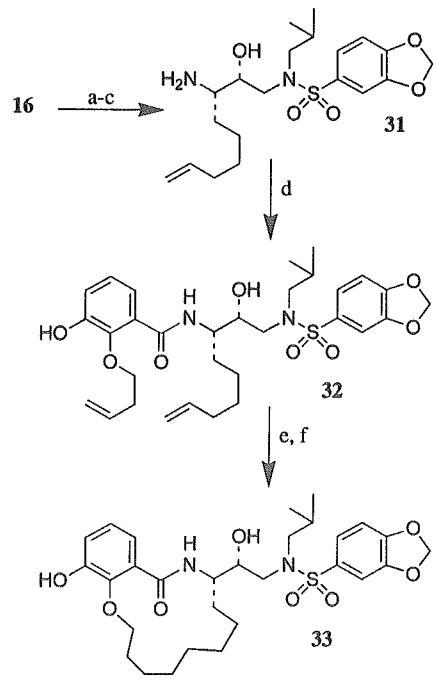

[a] Reagents and conditions: (a) $(CH_3)_2CHCH_2NH_2$, *i*PrOH, 90 °C. (b) 3,4-Methylenedioxybenzene sulfonyl chloride, CH_2Cl_2, aqueous $NaHCO_3$, 23 °C. (c) $LiAlH_4$, THF, 23 °C. (d) Acid **10**, EDC, HOBt, Et_3N, DMF, 23 °C. (e) Grubbs' cat. CH_2Cl_2, 23 °C. (f) H_2, 10% Pd–C, MeOH, 23 °C.

determinations. As can be seen, various saturated cycloamide-derived inhibitors have shown very impressive HIV-1 protease inhibitory activities. In general, the acyclic inhibitors were much less active than the corresponding macrocycles. Both 13-membered unsaturated inhibitor **22** and saturated inhibitor **30** with respective K_i values of 2 and 1 nM are significantly more

Table 1. Structure and Inhibitory Potencies of Various Acyclic and Cyclic Inhibitors

Entry No.	Compd	K_i (nM)
1.	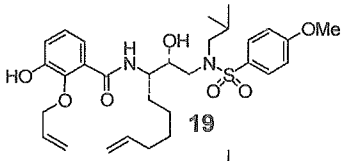 **19**	12
2.	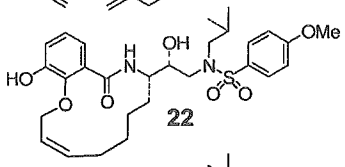 **22**	2 ± 0.15
3.	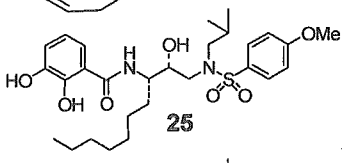 **25**	270
4.	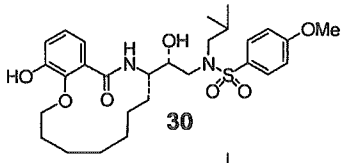 **30**	1 ± 0.16
5.	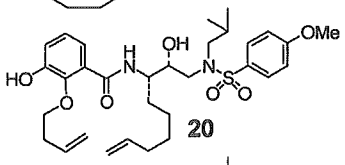 **20**	2 ± 0.13
6.	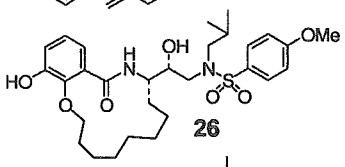 **26**	0.7 ± 0.1
7.	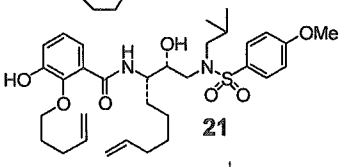 **21**	9 ± 1.2
8.	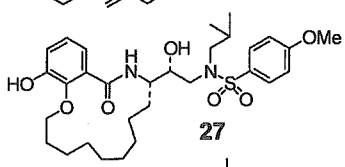 **27**	2 ± 0.28
9.	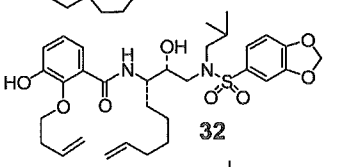 **32**	20
10.	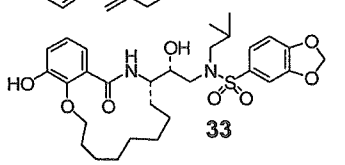 **33**	3 ± 0.33

potent as compared to acyclic inhibitor **19** with a K_i value of 12 nM. It is interesting to note the substantial loss in biological activity in the acyclic inhibitor **25** (K_i value of 270 nM) that resulted after cleavage of allylic ether. The 14-membered saturated macrocycle **26** with the *para*-methoxybenzenesulfonamide as the P_1' ligand is the most potent inhibitor in this series with a K_i value of 0.7 nM. The corresponding monounsaturated (inseparable 5:1 *cis–trans* olefins) compound mixture displayed

Table 2. Antiviral Activity of Selected Compounds against HIV-1_{LAI}

inhibitor	IC_{50} (μM)	IC_{75} (μM)
20	>1	>1
26	0.30 ± 0.11	0.74 ± 0.15
27	0.56 ± 0.33	>1
33	>1	>1
saquinavir	0.012 ± 0.006	0.047 ± 0.011
amprenavir	0.028 ± 0.009	0.079 ± 0.011

a K_i value of 1 nM. The 15-membered inhibitor **27** has shown nearly a 3-fold attenuation in potency as compared to the 14-membered inhibitor **26**. Because the 14-membered saturated cycloamide **26** was the most potent, we have investigated the substituent effects on the P_2' aromatic sulfonamide ring. In this context, we incorporated a 1,3-[benzo]dioxolane sulfonamide for the *para*-methoxybenzenesulfonamide. The inhibitory potency of the resulting saturated inhibitor **33** did not improve. The K_i value of the corresponding unsaturated macrocycle (inseparable 9:1 *cis–trans olefins*) was 4 nM, and the acyclic inhibitor **32** was significantly less potent.

We determined the antiviral activity of selected inhibitors. The results are summarized in Table 2. The IC_{50} and IC_{75} values shown were determined based on the inhibition of HIV-induced cytopathogenicity in MT-2 cells. All assays were conducted in duplicate, and the values with standard deviations denote the mean values from two or three. As can be seen, acyclic inhibitor **20** showed no antiviral activity. Inhibitors **26** and **27** (15-membered cycloamide) showed a moderate activity with antiviral IC_{50} values of about 0.3 and 0.55 μM, respectively. The antiviral activity of these compounds was substantially limited as compared to saquinavir[18] or amprenavir.[19] To improve antivitral potency, further modifications including incorporation of basic amine functionalities are in progress.

To gain insight into specific ligand-binding site interactions, an energy-minimized model structure of **26** was created (Figure 2). The structure was modeled in the active site of HIV-1 protease using the Molecular Operating Environment program (Chemical Computing Group, Montreal). The structure was built into the active site, based upon our published crystal structure of **1** complexed with HIV-1 protease (Protein Data Bank entry 1S6G) as a template.[6] The conformation and placement of the inhibitor was manually adjusted, and then, minimization was carried out using the force field[20] with the protease structure fixed. Finally, minimization was carried out with all atom positions relaxed.

Upon the basis of this model, it appears that the 3-hydroxyl group of P2-salicylic acid derivative is within an effective hydrogen-bonding distance to Asp-29 (3.3 Å) in the S_2 region of the active site. Also, the P2-carbonyl can effectively hydrogen bond to the tight-bound water molecule. The flexible macrocyclic carbon chain fills the S1–S2 hydrophobic pockets. Furthermore, the key hydrogen-bonding interaction of the P_2'-OMe group and the Asp-29′ is also quite apparent (distance 3.3 Å) as shown in Figure 2. However, the proper understanding of these active site interactions should await the solution of the X-ray crystal structure of a protein–ligand complex of **26**.[21]

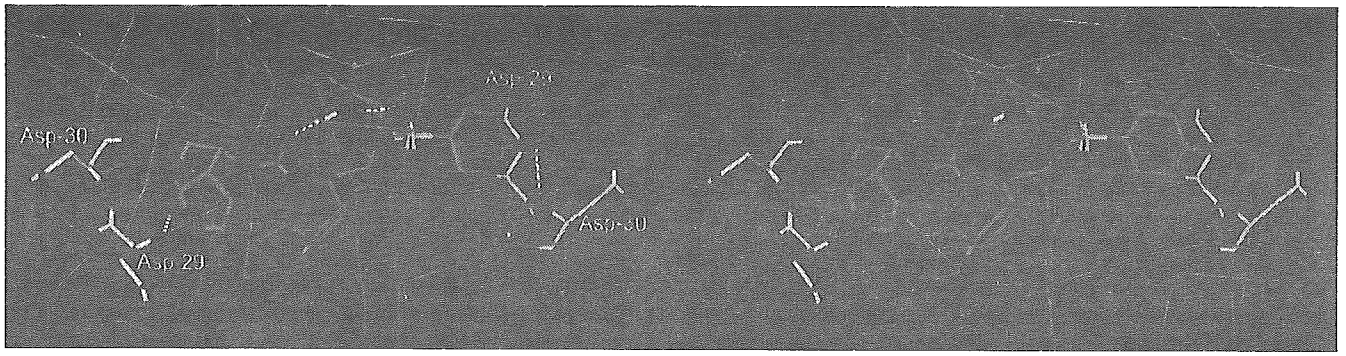

Figure 2. Stereoview of an energy minimized model structure of inhibitor **26** (magenta) overlayed with the inhibitor **1** (green)-bound crystal structure of HIV-1 protease.

Conclusion

A series of novel HIV protease inhibitors incorporating 3-hydroxysalicyclic acid-derived acyclic and cyclic P2 ligand has been designed, synthesized, and evaluated. The cyclic inhibitors incorporated 13−15-membered macrocycles. In general, cyclic inhibitors are considerably more potent than their acyclic counterparts both in enzyme inhibitory and in antiviral assays. Inhibitors with 13−15-membered macrocyclic ligands have shown subnanomolar enzyme inhibitory potencies. The inhibitors contain only two stereocenters, and the cyclic inhibitors can be readily prepared by using a ring-closing olefin metathesis. The saturated 14-membered macrocycle **26** with the *para*-methoxybenzenesulfonamide P_2' ligand displayed the highest enzyme inhibitory potency with a K_i value of 0.7 nM. This compound has also shown the best antiviral IC_{50} value of 0.3 μM. Substitution of a 1,3[benzo]dioxolane sulfonamide for the *para*-methoxybenzenesulfonamide resulted in a noticeable attenuation of biological activity of the 14-membered macrocycle. Further design and chemical modifications of these inhibitors utizing our structure-based design strategies are currently underway.

Experimental Section

General. ^{1}H and ^{13}C NMR spectra were obtained in $CDCl_3$ with an AM or Avance 400 Bruker instrument operating at 500 MHz for ^{1}H and 125 MHz for ^{13}C. Chemical shifts are reported in ppm, and coupling constants (J) are reported in Hertz. Optical rotations were measured using a Perkin-Elmer 341 polarimeter using a sodium lamp (589 nm) in chloroform unless otherwise stated. Infrared spectra were measured using a Genesis II FTIR in chloroform as thin films using sodium chloride plates. Thin-layer chromatography (TLC) was performed on E. Merck silica gel 60-F-254 plates. Mass spectra were recorded on a Finnegan LCQ mass spectrometer as the value *m/z*. Flash chromatography was performed using 230−400 mesh silica gel. Tetrahydrofuran was distilled from sodium/benzophenone, and benzene, methylene chloride, N,N-dimethylformamide, and toluene were distilled from CaH_2 under N_2.

3-(*tert*-Butyl-dimethyl-silanyloxy)-2-hydroxy-benzoic Acid Methyl Ester (5). To a stirring solution of 1.51 g (9.8 mmol) of 2,3-dihydroxybenzoic acid **4** in 35 mL of MeOH and 7 mL of water was added 1.60 g (4.9 mmol) of $CsCO_3$. The solution was stirred at 23 °C for 30 min and then concentrated. Absolute ethanol (3 × 4 mL) was added, the solution was reconcentrated to remove water, and the crude product was dried under vacuum. The resulting brown solid was dissolved in 10 mL of DMF, and the solution was cooled to 0 °C. Methyl iodide (0.64 mL, 10.3 mmol) was added, and after the solution was warmed to 23 °C, stirring was continued in the dark for 13 h. Water (40 mL) and EtOAc (70 mL) were added, and the layers were separated. The organic layer was then washed with water (3 × 40 mL) and then 40 mL of brine. The organic layer was dried over Na_2SO_4, filtered, and concentrated. The residue was purified by flash silica gel chromatography (5−20% EtOAc/hexanes) to provide the methyl ester as a pale yellow solid (1.33 g, 81%); mp 78−78.5 °C. IR (neat): 3463, 1675 cm^{-1}. ^{1}H NMR (400 MHz, $CDCl_3$): δ 10.90 (s, 1 H), 7.36 (dd, 1 H, J = 1.7, 8.2 Hz), 7.11 (dd, 1 H, J = 1.3, 8.0 Hz), 6.80 (t, 1 H, J = 7.9 Hz), 5.71 (s, 1 H), 3.95 (s, 3H). ^{13}C NMR (100 MHz, $CDCl_3$): δ 170.8, 148.8, 145.0, 120.6, 119.8, 119.2, 112.4, 52.5.

To a stirring solution of above ester (1.28 g, 7.6 mmol) in 6 mL of DMF at 0 °C was added 1.25 g (8.3 mmol) of TBDMSCl and 1.8 mL (10.3 mmol) of *N,N*-diisopropylethylamine. Stirring was continued at 0 °C for 20 min, and then, 35 mL of water and 45 mL of EtOAc were added. The layers were separated, and the organic layer was washed with 35 mL of water and 20 mL of brine, dried over Na_2SO_4, filtered, and concentrated. Purification by flash silica gel chromatography (hexanes to 5% EtOAc/hexanes) provided **5** as a yellow oil (2.07 g) 96%. IR (neat): 3173, 1679 cm^{-1}. ^{1}H NMR (500 MHz, $CDCl_3$): δ 10.76 (s, 1 H), 7.45 (dd, 1 H, J = 1.6, 8.1 Hz), 7.03 (dd, 1 H, J = 1.5, 8.0 Hz), 6.73 (t, 1 H, J = 8.0 Hz), 3.94 (s, 3 H), 1.01 (s, 9 H), 0.20 (s, 6 H). ^{13}C NMR (125 MHz, $CDCl_3$): δ 171.3, 154.3, 144.9, 126.7, 122.7. 118.9, 113.6, 52.7, 26.1, 18.9, −4.2.

2-Allyloxy-3-(*tert*-butyl-dimethyl-silanyloxy)benzoic Acid Methyl Ester (6). To a stirring solution of **5** (101 mg, 0.36 mmol) in 4 mL of THF was added 60 μL (0.381 mmol) of DEAD, 26 μL (0.382 mmol) of allyl alcohol, and 99.5 mg (0.379 mmol) of PPh_3. The solution was stirred at 23 °C for 3 h and then concentrated. Purification by flash silica gel chromatography (0.3−5% EtOAc/hexanes) provided the product **6** as a yellow oil in 58% yield. IR (neat): 2952, 1733, 1470 1299, 1020, 934, 836 cm^{-1}. ^{1}H NMR (500 MHz, $CDCl_3$): δ 7.37 (m, 1 H), 7.00 (m, 2 H), 6.11 (dddd, 1 H, J = 5.9, 5.9, 10.5, 17.2 Hz), 5.35 (ddd, 1 H, J = 1.6, 3.2, 17.2 Hz), 5.23 (ddd, 1 H, J = 1.2, 2.7, 10.4 Hz), 4.53 (ddd, 2 H, J = 1.2, 1.3, 5.9 Hz), 3.88 (s, 3 H), 1.01 (s, 9 H), 0.19 (s, 6 H). ^{13}C NMR (125 MHz, $CDCl_3$): δ 167.3, 150.4, 150.3, 134.5, 127.2, 125.3, 124.3, 124.0, 118.1, 74.8, 52.6, 26.1, 18.7, −4.1.

2-But-3-enyloxy-3-(*tert*-butyl-dimethyl-silanyloxy)benzoic Acid Methyl Ester (7). To a stirred solution of **5** (201 mg, 0.71 mmol) in 3 mL of THF was added 0.13 mL (0.83 mmol) of DEAD, 74 μL (0.86 mmol) of 3-buten-1-ol, and 226 mg (0.86 mmol) of PPh_3. The solution was stirred for 5 h and then concentrated. The crude product was purified by flash silica gel chromatography (0.5−4% EtOAc/hexanes) to give pure **7** as a yellow oil in 63% yield. IR (neat): 1734 cm^{-1}. ^{1}H NMR (500 MHz, $CDCl_3$): δ 7.34 (m, 1 H), 6.99 (m, 2 H), 5.88 (tdd, 1 H, J = 10.3, 13.6, 17.2 Hz), 5.13 (ddd, 1 H, J = 1.6, 3.2, 17.2 Hz), 5.06 (dd, 1 H, J = 1.5, 10.3 Hz), 4.05 (t, 2 H, J = 7.2 Hz), 3.89 (s, 3 H), 2.55 (m, 2 H), 1.01 (s, 9 H), 0.2 (s, 6 H). ^{13}C NMR (100 MHz, $CDCl_3$): δ 167.3, 150.5, 150.2, 135.1, 127.1, 125.1, 124.1, 123.9, 117.1, 73.2, 52.5, 34.9, 26.1, 18.7, −4.0.

3-(*tert*-Butyl-dimethyl-silanyloxy)-2-pent-4-enyloxy-benzoic Acid Methyl Ester (8). Etherification of **5** with

4-penten-1-ol following the procedure for **6** provided 160 mg of **8** in 89% yield as a colorless oil. IR (neat): 1733 cm^{-1}. ^1H NMR (500 MHz, $CDCl_3$): δ 7.33 (dd, 1 H, J = 2.9, 6.6 Hz), 6.98 (m, 2 H), 5.86 (tdd, 1 H, J = 6.6, 10.3, 17.2 Hz), 5.04 (ddd, 1 H, J = 1.6, 3.4, 17.1 Hz), 4.97 (dd, 1 H, J = 1.6, 10.2 Hz), 4.01 (t, 2 H, J = 7.0 Hz), 3.89 (s, 3 H), 2.19 (m, 2 H), 1.89 (m, 2 H), 1.01 (s, 9 H), 0.20 (s, 6 H). ^{13}C NMR (125 MHz, $CDCl_3$): δ 167.4, 150.7, 150.2, 138.7, 127.1, 125.1, 124.0, 123.8, 115.1, 73.8, 52.5, 30.6, 29.7, 26.1, 18.7, −4.0.

2-Allyloxy-3-hydroxy-benzoic Acid (9). To a stirring solution of 113 mg of **6** in 4 mL of THF at 0 °C was added 0.56 mL of TBAF (1 M THF) dropwise under N_2. Stirring was continued at 0 °C for about 10 min after which time 10 mL of saturated NH_4Cl solution, 4 mL of water, and 15 mL of EtOAc were added. The layers were separated, and the organic layer was washed with 15 mL of water and then 15 mL of brine, dried over Na_2SO_4, filtered, and concentrated. Purification by flash silica gel chromatography (2−5% EtOAc/hexanes) resulted in 56.2 mg (0.349 mmol) of the corresponding methyl ester in 77% yield as a colorless oil. IR (neat): 3420, 2952, 1722, 1466, 1284, 988, 755 cm^{-1}. ^1H NMR (500 MHz, $CDCl_3$): δ 7.41 (dd, 1 H, J = 1.7, 7.9 Hz), 7.15 (dd, 1 H, J = 1.7, 8.1 Hz), 7.06 (t, 1 H, J = 8.0 Hz), 6.10 (qdd, 1 H, J = 6.0, 6.1, 10.4 Hz), 5.96 (s, 1 H), 5.43 (m, 1 H), 5.32 (dd, 1 H, J = 0.69, 10.3 Hz), 4.53 (d, 2 H, J = 6.1 Hz), 3.91 (s, 3 H). ^{13}C NMR (125 MHz, $CDCl_3$): δ 166.3, 150.4, 146.2, 133.6, 124.9, 124.2, 123.2, 119.9, 119.8, 76.6, 52.7.

A mixture of the above ester (30.7 mg, 0.15 mmols) and 32.7 mg (0.78 mmols) of LiOH in 2 mL of THF and 2 mL of water was stirred at 55 °C for 2.5 h. Heating was stopped, and 2 mL of 1 N HCl, 2 mL of water, and 8 mL of EtOAc were added. After the layers were separated, the organic layer was washed with 5 mL of brine, dried over sodium sulfate, filtered, and concentrated. Purification by flash silica gel chromatography of the crude product resulted in 23.6 mg of acid **9** in 83% yield as a colorless solid; mp 101.5−103.5 °C. IR (neat): 3162, 1703, 1417, 1295, 1210, 944, 747 cm^{-1}. ^1H NMR (500 MHz, $CDCl_3$): δ 7.62 (dd, 1 H, J = 1.7, 7.9 Hz), 7.20 (dd, 1 H, J = 1.7, 8.0 Hz), 7.13 (t, 1 H, J = 8.0), 6.13 (tdd, 1 H, J = 6.2, 10.5, 16.9 Hz), 5.46 (m, 1 H), 5.38 (dd, 1 H, J = 0.6, 9.7 Hz), 4.64 (d, 2 H, J = 6.2 Hz). ^{13}C NMR (125 MHz, $CDCl_3$): δ 167.5, 149.8, 146.2, 132.6, 125.6, 124.5, 123.1, 121.7, 121.2, 76.9.

2-But-3-enyloxy-3-hydroxy-benzoic Acid (10). To 129 mg (0.38 mmol) of **7** in 3 mL of THF at 0 °C with stirring was added slowly 0.6 mL of TBAF (1 M THF). After 20 min, 10 mL of saturated NH_4Cl solution, 2 mL of water, and 15 mL of EtOAc were added. The organic layer was washed with 10 mL of brine, dried over Na_2SO_4, filtered, and concentrated. Purification by flash silica gel chromatography (5−10% EtOAc/hexanes) gave 65 mg of the corresponding diol in 77% yield as a colorless oil. IR (neat): 3443, 1726 cm^{-1}. ^1H NMR (400 MHz, $CDCl_3$): δ 7.39 (dd, 1 H, J = 1.7, 7.7 Hz), 7.13 (dd, 1 H, J = 1.7, 8.1 Hz), 7.04 (t, 1 H, J = 8.0 Hz), 6.08 (s, 1 H), 5.95 (tdd, 1 H, J = 6.9, 10.2, 17.2 Hz), 5.30 (ddd, 1 H, J = 1.5, 2.8, 16.9 Hz), 5.24 (dd, 1 H, J = 1.1, 9.7 Hz), 4.08 (t, 2 H, J = 6.1 Hz), 3.92 (s, 3 H), 2.55 (m, 2 H). ^{13}C NMR (100 MHz, $CDCl_3$): δ 166.4, 150.4, 146.5, 135.3, 124.8, 124.0, 123.1, 119.9, 119.0, 74.5, 52.6, 35.0.

A mixture of above diol (61 mg, 0.28 mmol) and 79 mg (1.9 mmols) of LiOH in 2 mL of THF and 2 mL of water was heated at 55 °C. After 2 h, 2 mL of 1 N HCl and 15 mL of EtOAc were added. The layers were separated, and the organic layer was washed with 10 mL of brine, dried over Na_2SO_4, filtered, and concentrated. Purification by flash silica gel chromatography (10% MeOH/CH_2Cl_2) provided **10** in 94% yield (54 mg) as a white solid; mp 70−73 °C. IR (neat): 3177, 1716 cm^{-1}. ^1H NMR (400 MHz, $CHCl_3$): δ 7.58 (d, 1 H, J = 7.7 Hz), 7.19 (d, 1 H, J = 7.9 Hz), 7.11 (t, 1 H, J = 7.9 Hz), 5.95 (m, 1 H), 5.29 (m, 2 H), 4.17 (t, 2 H, J = 6.1 Hz), 2.58 (m, 2 H). ^{13}C NMR (100 MHz, $CHCl_3$) δ 168.9, 149.7, 146.4, 134.4, 124.9, 123.8, 122.4, 121.1, 119.0, 74.5, 34.4.

3-Hydroxy-2-pent-4-enyloxy-benzoic Acid (11). A mixture of 160 mg (0.45 mmol) of **8** and 111 mg (2.64 mmol) of LiOH in 6 mL of THF and 2 mL of water was stirred at 23 °C for about 2 h and then at 50 °C for 12.5 h. Heating was stopped, and 1 N HCl was added to a pH of 1 followed by 12 mL of EtOAc. The layers were separated, and the organic layer was washed wih 5−6 mL of brine, dried over Na_2SO_4, filtered, and concentrated. Purification by flash silica gel chromatography (20−50% EtOAc/hexanes) gave pure product **11** as a white amorphous solid; 89 mg in 88% yield; mp 70−74 °C. IR (neat): 3082, 1702 cm^{-1}. ^1H NMR (500 MHz, $CHCl_3$): δ 7.58 (dd, 1 H, J = 1.6, 7.9 Hz), 7.21 (dd, 1 H, J = 1.5, 8.1 Hz), 7.09 (t, 1 H, J = 8.0 Hz), 5.87 (tdd, 1 H, J = 6.7, 10.3, 17.1 Hz), 5.04 (dd, 2 H, J = 1.4, 10.2 Hz), 4.13 (t, 2 H, J = 6.6 Hz), 2.27 (q, 2 H, J = 7.1 Hz), 1.97 (quint, 2 H, J = 7.0 Hz). ^{13}C NMR (125 MHz, $CDCl_3$): δ 169.9, 150.1, 146.9, 138.1, 125.2, 124.2, 122.8, 121.8, 116.1, 75.6, 30.5, 29.5.

(*E*)-Nona-2,8-dien-1-ol (13). To a stirring solution of diol **12** (1.36 g, 9.5 mmol) in 10 mL of THF and 1 mL of water was added 5.29 g (24.7 mmol) of $NaIO_4$. The resulting white mixture was stirred at 23 °C for about 30 min. The mixture was dried with Na_2SO_4, filtered through Celite, and concentrated. The resulting aldehyde was again dried with Na_2SO_4, concentrated, and used without further purification for the next reaction.

To a stirring solution of triethylphosphonoacetate (2.43 g, 10.8 mmols) in 6 mL of THF at 0 °C was added 436 mg of NaH (60% dispersion in mineral oil). After 20 min, the above aldehyde was added in 6 mL of THF, and the solution was allowed to warm to 23 °C. After 15 min, the reaction was quenched with about 2 mL of saturated NH_4Cl solution and 1 mL of water. Diethyl ether (15 mL) was added, and the layers were separated. The organic layer was washed with 10 mL of brine, dried over Na_2SO_4, filtered, and concentrated. Purification (flash silica gel chromatography-hexanes to 2% EtOAc/hexanes) gave the corresponding α,β-unsaturated ester (1.36 g, 79%) as a pale yellow liquid. IR (neat): 1722, 1654 cm^{-1}. ^1H NMR (400 MHz, $CDCl_3$): δ 6.96 (ddd, 1 H, J = 6.9, 7.0, 15.6 Hz), 5.80 (m, 2 H), 5.00 (ddd, 1 H, J = 1.6, 3.2, 17.0 Hz), 4.95 (dd, 1 H, J = 1.1, 9.7 Hz), 4.18 (q, 2 H, J = 7.1 Hz), 2.20 (m, 2 H), 2.06 (q, 2 H, J = 7.0 Hz), 1.45 (m, 4 H), 1.29 (t, 3 H, J = 7.2 Hz). ^{13}C NMR (400 MHz, $CDCl_3$): δ 166.8, 149.2, 138.6, 121.3, 114.6, 60.1, 33.5, 32.0, 28.3, 27.4, 14.3.

To a stirred solution of the above ester (1.32 g, 7.2 mmol) in 20 mL of CH_2Cl_2 at −78 °C was added 17 mL of DIBAL-H (1 M hexanes). After it was stirred at −78 °C for 20 min, 20 mL of EtOAc and 40 mL of 1 N HCl were added, and after this mixture was warmed to 23 °C, 140 mL of 1 N HCl and 20 mL of CH_2Cl_2 were added. The layers were separated, dried over Na_2SO_4, filtered, and concentrated. Purification by flash silica gel chromatograghy (10% EtOAc/hexanes) provided **13** as a pale yellow liquid in 90% yield (910 mg). IR (neat): 3336 cm^{-1}. ^1H NMR (400 MHz, $CDCl_3$): δ 5.81 (tdd, 1 H, J = 6.7, 10.3, 17.3), 5.66 (dtd, 2 H, J = 5.8, 15.3, 20.2), 5.00 (ddd, 1 H, J = 1.7, 3.4, 16.9 Hz), 4.93 (m, 1 H), 4.08 (d, 2 H, J = 5.1 Hz), 2.05 (m, 4 H), 1.39 (m, 4 H), 1.31 (s, 1 H). ^{13}C NMR (100 MHz, $CDCl_3$): δ 138.9, 133.3, 129.0, 114.4, 63.8, 33.6, 32.0, 28.6, 28.4.

(2*R*,3*R*)-(3-Hex-5-enyl-oxiranyl)methanol (14). A 125 mL reaction flask with 183 mg of 4 Å molecular sieves powder was flame-dried and cooled under vacuum. To the flask was added 20 mL of CH_2Cl_2, followed by 0.10 mL (0.34 mmol) of $Ti(O^iPr)_4$ and 60 μL (0.055 mmol) of (−)-DET. The resulting solution was cooled to −20 °C, and 2.0 mL of *tert*-butyl hydroperoxide (5−6 M decane) was added dropwise. After 45 min, 0.887 g (6.3 mmol) of **13** in 10 mL of CH_2Cl_2 was added and stirring was continued at −20 °C for 3 h and was aged in a refrigerator for 11 h at about −20 °C. The solution mixture was warmed to 0 °C, and 3 mL of water was added. After 30 min, a 30% NaOH/brine solution was added, and the mixture was warmed to 23 °C. After 1 h, 20 mL of CH_2Cl_2 was added, and the layers were separated. The aqueous layer was extracted with 10 mL of CH_2Cl_2, and the combined extracts were dried over Na_2SO_4. Purification by flash silica gel chromatography (20−25% EtOAc/hexanes) gave 0.798 g of **14** in 78% yield as a pale yellow liquid: $[\alpha]_D^{23}$ +34.2 (*c* 0.30, $CHCl_3$). IR (neat): 3400, 1026 cm^{-1}. ^1H NMR (400 MHz, $CDCl_3$): δ 5.80 (tdd, 1 H, J = 6.8, 10.3, 17.1 Hz), 5.00 (ddd, 1

H, J = 1.7, 3.5, 17.2 Hz), 4.95 (dd, 1 H, J = 1.0, 9.5 Hz), 3.91 (ddd, 1 H, J = 2.6, 5.6, 12.5 Hz), 3.63 (m, 1 H), 2.96 (ddd, 1 H, J = 2.4, 5.5, 5.7 Hz), 2.92 (ddd, 1 H, J = 2.1, 2.5, 4.5 Hz), 2.06 (m, 2 H), 1.8 (m,1 H), 1.57 (m, 2 H), 1.46 (m, 4 H). ^{13}C NMR (100 MHz, $CDCl_3$): δ 138.6, 114.6, 61.6, 58.4, 55.9 33.6, 31.4, 28.6, 25.4.

(2*S*,3*S*)-3-Azido-non-8-ene-1,2-diol (15). A solution of 1.5 mL (5.1 mmol) of $Ti(O^iPr)_4$ and 1.2 mL (9.0 mmol) of $TMSN_3$ in 20 mL of benzene was heated at 90 °C for 4 h. To the heating yellow solution was added 0.77 g (4.9 mmol) of **14** in 5 mL of benzene, and reflux was continued for 20 min. The solution was then cooled to 0 °C, 40 mL of 15% H_2SO_4 solution was added, and the mixture was stirred vigorously for 1 h. The layers were separated, and the organic layer was washed with 20 mL of saturated $NaHCO_3$ solution, then with 20 mL of brine, dried over Na_2SO_4, filtered, and concentrated. Purification by flash silica gel chromatography (40% EtOAc/hexanes) provided **15** as a yellow oil in 100% yield (0.97 g): $[\alpha]_D^{23}$ +13.2 (*c* 0.49, $CHCl_3$). IR (neat): 3077, 2101 cm^{-1}. ^{1}H NMR (400 MHz, $CDCl_3$): δ 5.80 (ddd, 1 H, J = 6.6, 10.1, 16.8 Hz), 4.99 (m, 2 H), 3.72 (m, 3 H), 3.46 (m, 1 H), 2.80 (s, 1 H), 2.09 (m, 3 H), 1.54 (m, 6 H). ^{13}C NMR (100 MHz, $CDCl_3$): δ 138.5, 114.7, 73.5, 64.6, 63.1, 33.5, 30.4, 28.6, 25.7. MS-ESI (*m/z*): 222.2 $(M + Na)^+$.

(1*S*,2′*R*)-2′-(1-Azido-hept-6-enyl)oxirane (16). A clear solution of (960 mg, 4.8 mmol) of **15** and 1-chlorocarbonyl-methylethyl acetate (0.9 mL, 0.62 mmol) in 10 mL of $CHCl_3$ was stirred at 23 °C for 15 min. Saturated $NaHCO_3$ solution was added, and the mixture was stirred for 10 min. The layers were separated, and the organic layer was dried over Na_2SO_4, filtered, and concentrated. The crude product was used directly for the next reaction without further purification.

A mixture of the above crude product and NaOMe (0.37 g, 6.8 mmol) in 10 mL of THF was stirred at 23 °C for 3 h. To the mixture was added 6 mL of saturated NH_4Cl solution, 2 mL of water, and 20 mL of EtOAc. The layers were separated, and the organic layer was dried over Na_2SO_4, filtered, and concentrated. The crude product was purified by flash silica gel chromatography (5% EtOAc/hexanes) to give 2.60 g and 54% yield of **16** as a yellow oil: $[\alpha]_D^{23}$ +5.9 (*c* 0.32, $CHCl_3$). IR (neat): 2101 cm^{-1}. ^{1}H NMR (400 MHz, $CDCl_3$): δ 5.80 (tdd, 1 H, J = 6.7, 10.3, 17.2 Hz), 4.99 (m, 2 H), 3.32 (m, 1 H), 3.01 (m, 1 H), 2.80 (m, 2 H), 2.08 (m, 2 H), 1.80−1.41 (m, 6 H). ^{13}C NMR (100 MHz, $CDCl_3$): δ 138.5, 114.7, 62.5, 53.4, 44.9, 33.5, 31.7, 28.6, 25.2.

(2*R*,3*S*)-*N*-(3-Azido-2-hydroxy-non-8-enyl)-*N*-isobutyl-4-methoxy-benzenesUlfonamide (17). A solution of **16** (0.45 g, 2.5 mmol) and isopropylamine (0.41 mL, 4.1 mmol) in 5 mL of ^{i}PrOH was stirred at 90 °C for 80 min. After this period, the reaction mixture was concentrated. The residue was purified by flash silica gel chromatography (60−80% EtOAc/hexanes) to provide the corresponding amine as a yellow oil (0.38 g, 62%): $[\alpha]_D^{23}$ +2.0 (*c* 0.45, $CHCl_3$). IR (neat): 3323, 2100 cm^{-1}. ^{1}H NMR (500 MHz, $CDCl_3$): δ 5.80 (tdd, 1 H, J = 6.7, 10.3, 17.1 Hz), 5.01 (ddd, 1 H, J = 1.6, 3.4, 17.1 Hz), 4.95 (dd, 1 H, J = 1.8, 10.1 Hz), 3.58 (ddd, 1 H, J = 3.7, 5.3, 12.6 Hz), 3.39 (m, 1 H), 2.77 (dd, 1 H, J = 3.6, 12.1 Hz), 2.64 (dd, 1 H, J = 8.9, 12.1 Hz), 2.43 (ddd, 3 H, J = 6.8, 9.0, 11.7 Hz), 2.07 (dd, 2 H, J = 7.0 Hz), 1.72 (octet, 1 H, J = 6.7 Hz), 1.63−1.51 (m, 2 H), 1.51−1.40 (m, 5 H), 0.92 (d, 3 H, J = 2.1 Hz), 0.91 (d, 3 H, J = 2.1 Hz). ^{13}C NMR (125 MHz, $CDCl_3$): δ 139.0, 115.0, 71.3, 66.1, 58.0, 50.8, 34.0, 30.8, 29.0, 28.9, 26.3, 20.9.

A mixture of above amine (88 mg, 0.34 mmol) and 4-methoxybenzenesulfonyl chloride (70.9 mg, 0.34 mmol) in a mixture (1:1) of CH_2Cl_2 and saturated $NaHCO_3$ solution (10 mL) was stirred at 23 °C. After 12.5 h, 10 mL of CH_2Cl_2 was added, and the layers were separated. The aqueous layer was extracted with 10 mL of CH_2Cl_2. The combined extracts were dried over Na_2SO_4, filtered, and concentrated. The crude product was purified by flash silica gel chromatography to give **17** (132 mg, 90%) as a clear oil: $[\alpha]_D^{23}$ −19.6 (*c* 0.5, $CHCl_3$). IR (neat): 3498, 2101, 1597, 1335 cm^{-1}. ^{1}H NMR (400 MHz, $CDCl_3$): δ 7.76 (dd, 1 H, J = 3.0, 9.9 Hz), 7.75 (dd, 1 H, J = 2.0, 7.0 Hz), 7.02 (dd, 1 H, J = 2.9, 10.1 Hz), 7.01 (dd, 1 H, J = 1.7, 7.2 Hz), 5.80 (tdd, 1 H, J = 6.7, 10.3, 17.0 Hz), 5.01 (dd, 1 H, J = 1.6, 17.2 Hz), 4.96 (d, 1 H, J = 10.4 Hz), 3.88 (s, 3 H), 3.78 (m, 1 H), 3.47 (d, 1 H, J = 3.1 Hz), 3.34 (ddd, 1 H, J = 3.7, 5.5, 8.7 Hz), 3.21 (dd, 1 H, J = 9.4, 15.3 Hz), 3.02 (m, 2 H), 2.81 (dd, 1 H, J = 6.5, 13.3 Hz), 2.08 (q, 2 H, J = 6.8 Hz), 1.85 (m, 1 H), 1.65 (m, 1 H), 1.60−1.42 (m, 5 H), 0.96 (d, 3 H, J = 6.6 Hz), 0.90 (d, 3 H, J = 6.6 Hz). ^{13}C NMR (100 MHz, $CDCl_3$): δ 163.1, 138.5, 129.7, 129.5, 114.7, 114.4, 72.4, 65.4, 58.9, 55.6, 52.7, 33.5, 30.3, 28.6, 27.2, 25.6, 20.2, 19.8. MS-ESI (*m/z*): 425.2 $(M + H)^+$.

(2*R*,3*S*)-*N*-(3-Amino-2-hydroxy-non-8-enyl)-*N*-isobutyl-4-methoxy-benzeneSulfonamide (18). To a stirred suspension of $LiAlH_4$ (20 mg, 0.25 mmol) in 5 mL of THF was added **17** (110 mg, 0.24 mmol) in 5 mL of THF. Stirring was continued for 50 min, and the reaction was quenched by adding successively 20 μL of water, 20 μL of 15% NaOH, and 60 μL of brine. The mixture was filtered through Celite and concentrated. The resulting product **18** was used in the next reaction without further purification. IR (neat): 3351, 1596, 1333 cm^{-1}. ^{1}H NMR (400 MHz, $CDCl_3$): δ 7.75 (dd, 1 H, J = 2.9, 11.7 Hz), 7.74 (dd, 1 H, J = 1.7, 7.1 Hz), 6.98 (dd, 1 H, J = 2.9, 11.8 Hz), 6.97 (dd, 1 H, J = 1.9, 7.1 Hz), 5.79 (tdd, 1 H, J = 6.6, 10.2, 17.2 Hz), 5.02 (ddd, 1 H, J = 1.6, 3.3, 17.0 Hz), 4.94 (m, 1 H), 3.87 (s, 3 H), 3.70 (m, 1 H), 3.25 (dd, 1 H, J = 9.3, 15.0 Hz), 3.04 (m, 2 H), 2.85 (m, 2 H), 2.06 (dd, 2 H, J = 6.7, 13.5 Hz), 1.90 (m, 2 H), 1.50−1.30 (m, 5 H), 1.43 (m, 3 H), 0.94 (d, 3 H, J = 6.5 Hz), 0.90 (d, 3 H, J = 6.5 Hz). ^{13}C NMR (125 MHz, $CDCl_3$): δ 163.3, 139.1, 130.7, 129.9, 115.0, 114.7, 73.6, 58.9, 56.0, 54.8, 52.4, 34.1, 33.1, 29.3, 27.6, 26.3, 20.6, 20.3.

(1′*S*,1″*R*)-2-Allyloxy-3-hydroxy-*N*-(1′-{1″-hydroxy-2″-[isobutyl-(4-methoxy-benzenesulfonyl)amino]ethyl}hept-6′-enyl)benzamide (19). To a stirring solution of acid **9** (23.9 mg, 0.12 mmol) in 2 mL of DMF at 0 °C was added EDC (30.1 mg, 0.16 mmol), HOBt (22.2 mg, 0.16 mmol), 50.8 mg (0.127 mmol) of amine **18** in 2 mL of DMF, and 86 μL (0.62 mmol) of Et_3N. The solution was allowed to warm to 23 °C, and stirring was continued for 19 h. To this solution was then added 4 mL of water and 20 mL of EtOAc. The layers were separated, and the organic layer was washed with 10 mL of water and 10 mL of brine, dried over Na_2SO_4, filtered, and concentrated. Flash silica gel chromatography yielded **19** (35.1 mg, 50%) as an oil: $[\alpha]_D^{23}$ −12.5 (*c* 0.12, $CHCl_3$). IR (neat): 3347, 2926, 1638, 1577, 1534, 1497, 1463, 1334, 1260, 1151, 1091, 807, 757 cm^{-1}. ^{1}H NMR (400 MHz, $CDCl_3$): δ 7.70 (m, 3 H), 7.52 (dd, 1 H, J = 2.8, 6.7 Hz), 7.12 (m, 2 H), 6.96 (d, 2 H, J = 8.9 Hz), 6.11 (m, 1 H), 5.77 (tdd, 1 H, J = 6.6, 10.3, 17.1 Hz), 5.64 (s, 1 H), 5.48 (d, 1 H, J = 17.1 Hz), 5.37 (d, 1 H, J = 10.5 Hz), 4.97 (dd, 1 H, J = 1.6, 15.5 Hz), 4.92 (d, 1 H, J = 10.4 Hz), 4.55 (dd, 1 H, J = 5.8, 12.4 Hz), 4.45 (dd, 1 H, J = 5.8, 12.4 Hz), 4.10 (m, 1 H), 3.93 (dd, 1 H, J = 3.2, 9.1 Hz), 3.87 (s, 3 H), 3.78 (d, 1 H, J = 3.4 Hz), 3.18 (dd, 1 H, J = 9.0, 15.2 Hz), 3.04 (d, 1 H, J = 2.4 Hz), 2.98 (dd, 1 H, J = 8.4, 13.4 Hz), 2.84 (dd, 1 H, J = 6.8, 13.3 Hz), 2.04 (m, 2 H), 1.86 (m, 1 H), 1.63 (m, 2 H), 1.44 (m, 2 H), 1.38 (m, 2 H), 0.91 (d, 3 H, J = 6.6 Hz), 0.86 (d, 3 H, J = 6.5 Hz). ^{13}C NMR (125 MHz, $CDCl_3$): δ 165.8, 163.4, 149.6, 144.0, 139.1, 132.7, 130.4, 129.9, 127.3, 125.8, 122.9, 120.2, 119.6, 115.0, 114.7, 76.3, 73.5, 58.9, 56.0, 54.0, 53.4, 34.0, 30.1, 29.5, 29.3, 27.6, 26.1, 20.5, 20.3. HRMS-ESI (*m/z*): $(M + Na)^+$ calcd for $C_{30}H_{42}N_2O_7NaS$, 574.2713; found, 574.2792.

(1″*S*,1‴*R*)-2-But-3′-enyloxy-3-hydroxy-N-(1″-{1‴-hydroxy-2‴-[isobutyl-(4-methoxy-benzenesulfonyl)amino]-ethyl}hept-6″-enyl)benzamide (20). To a stirring solution of 52 mg (0.12 mmol) of amine **18** in 2 mL of DMF at 0 °C was added 25 mg (0.13 mmol) of EDC, 16 mg (0.12 mmol) of HOBt, 20 mg (0.096 mmol) of acid **10** in 2 mL of DMF, and finally 66 μL (0.47 mmol) of triethylamine. The mixture was allowed to warm to 23 °C, and stirring was continued for 9 h. Water (5 mL) and EtOAc (20 mL) were added, and the layers were separated. The organic layer was washed with 5 mL of water and 6 mL of brine, dried over Na_2SO_4, filtered, and concentrated. Purification by flash silica gel chromatography (40% EtOAc/hexanes) provided **20** (34.1 mg) as an oil (61%): $[\alpha]_D^{23}$ −12.9 (*c* 0.19, $CHCl_3$). IR (neat): 3339, 1638, 1577, 1535, 1334

cm^{-1}. ^{1}H NMR (500 MHz, $CDCl_3$): δ 7.73 (m, 3 H), 7.48 (dd, 1 H, J = 2.3, 7.3 Hz), 7.10 (m, 2 H), 6.98 (dd, 1 H, J = 2.9, 11.9 Hz), 6.97 (dd, 1 H, J = 2.0, 6.9 Hz), 5.96 (tdd, 1 H, J = 6.9, 10.2, 17.2 Hz), 5.83 (s, 1 H) 5.77 (tdd, 1 H, J = 6.7, 10.3, 17.1, Hz), 5.33 (m, 1 H), 5.29 (d, 1 H, J = 10.2 Hz), 4.97 (ddd, 1 H, J = 1.7, 3.5, 17.0 Hz), 4.91 (m, 1 H), 4.09 (m, 2 H), 3.95 (m, 2 H), 3.87 (s, 3 H), 3.80 (d, 1 H, J = 3.2, Hz), 3.21 (dd, 1 H, J = 9.1, 15.1 Hz), 3.01 (m, 1 H), 2.98 (dd, 1 H, J = 2.9, 5.6 Hz), 2.83 (dd, 1 H, J = 6.6, 13.3 Hz), 2.57 (m 2 H), 2.04 (m, 2 H), 1.86 (m, 1 H), 1.60 (m, 2 H), 1.45 (m, 2 H), 1.38 (m, 2 H), 0.91 (d, 3 H, J = 6.6 Hz), 0.86 (d, 3 H, J = 6.6 Hz). ^{13}C NMR (125 MHz, $CDCl_3$): δ 165.9, 163.5, 149.6, 144.3, 139.1, 134.6, 130.3, 129.9, 127.3, 125.8, 122.6, 119.7, 119.5, 115.0, 114.8, 74.8, 73.5, 59.1, 56.0, 54.1, 53.2, 34.6, 34.0, 30.1, 29.3, 27.6, 26.1, 20.5, 20.3. MS-ESI (*m/z*): 589.2 (M + H)$^+$. HRMS-ESI (*m/z*) [M + Na]$^+$ calcd for $C_{31}H_{44}N_2O_7NaS$, 611.2769; found, 611.2767.

(1″*S*,1‴*R*)-3-Hydroxy-N-(1″-{1‴-hydroxy-2‴-[isobutyl-(4-methoxy-benzenesulfonyl)amino]ethyl}hept-6″-enyl)-2-pent-4‴″-enyloxy-benzamide (21). Acid **11** was coupled with amine **18** according to the general procedure for **20** to give **21** (39 mg, 76%) as an oil: $[\alpha]_D^{23}$ −15.3 (*c* 0.15, $CHCl_3$). IR (neat): 3347, 1638, 1577, 1535, 1335 cm^{-1}. ^{1}H NMR (500 MHz, $CDCl_3$): δ 7.77 (d, 1 H, J = 8.6 Hz), 7.73 (dd, 1 H, J = 2.9, 11.9 Hz), 7.71 (dd, 1 H, J = 2.0, 6.9 Hz), 7.51 (dd, 1 H, J = 2.9, 6.7 Hz), 7.10 (m, 2 H), 6.98 (dd, 1 H, J = 2.9, 11.8 Hz), 6.97 (dd, 1 H, J = 2.0, 6.9 Hz), 5.89 (tdd, 1 H, J = 6.7, 10.2, 17.1 Hz), 5.77 (tdd, 1 H, J = 6.7, 10.3, 17.0 Hz), 5.71 (s, 1 H), 5.15 (ddd, 1 H, J = 1.6, 3.2, 17.2 Hz), 5.08 (dd, 1 H, J = 1.5, 10.1 Hz), 4.98 (ddd, 1 H, J = 1.6, 3.4, 17.1 Hz), 4.92 (m, 1 H), 4.09 (m, 1 H), 4.01 (m, 1 H), 3.93 (m, 2 H), 3.87 (s, 3 H), 3.78 (d, 1 H, J = 3.2 Hz), 3.21 (dd, 1 H, J = 9.1, 15.1 Hz), 3.01 (d, 1 H, J = 1.9 Hz), 2.98 (m, 1 H), 2.83 (dd, 1 H, J = 6.6, 13.2 Hz), 2.29 (q, 2 H, J = 7.0 Hz), 2.03 (m, 2 H), 1.98 (quint., 2 H, J = 7.0 Hz), 1.85 (m, 1 H), 1.63 (m, 2 H), 1.45 (m, 2 H), 1.38 (m, 2 H), 0.91 (d, 3 H, J = 6.6 Hz), 0.86 (d, 3 H, J = 6.6 Hz). ^{13}C NMR (125 MHz, $CDCl_3$): δ 165.8, 163.4, 149.6, 144.4, 139.1, 138.3, 130.3, 129.9, 127.1, 125.7, 122.9, 119.6, 116.3, 115.0, 114.8, 75.5, 73.5, 59.0, 56.0, 54.1, 53.2, 34.0, 30.7, 30.1, 29.4, 29.3, 27.6, 26.1, 20.5, 20.3. HRMS-ESI (*m/z*): (M + Na)$^+$ calcd for $C_{32}H_{46}N_2O_7NaS$, 625.2934; found, 625.2923.

(2″*R*,13*S*)-N-[2′Hydroxy-2″-(4-hydroxy-15-oxo-6,9,10,-11,12,13,14,15-octahydro-5-oxa-14-aza-benzocyclotridecen-13-yl)ethyl]-N-isobutyl-4-methoxy-benzenesulfonamide (22). To a stirred solution of **19** (29.3 mg, 0.05 mmol) in 20 mL of CH_2Cl_2 was added 4.2 mg (0.0051 mmol) of Grubbs' catalyst. The solution was allowed to stir for 45 min under Ar and then concentrated. Flash silica gel chromatography (40 to 45% EtOAc/ hexanes) resulted in **22** (26.8 mg, 96%) as a pale yellow foam as a mixture (5.5:1). IR (neat): 3341, 2953, 1635, 1575, 1538, 1463, 1333, 1260, 1152, 1091, 756 cm^{-1}. ^{1}H NMR of trans diastereomer (400 MHz, $CDCl_3$): δ 8.13 (d, 1 H, J = 9.2 Hz), 7.66 (m, 2 H), 7.09 (d, 2 H, J = 4.8 Hz), 6.90 (d, 2 H, J = 8.8 Hz), 5.75 (m, 2 H), 5.35 (s, 1 H), 4.99 (dd, 1 H, J = 6.4, 11.2 Hz), 4.27 (dd, 1 H, J = 7.2, 11.2 Hz), 4.00 (m, 1 H), 3.84 (s, 3 H), 3.81 (m, 1 H), 3.61 (d, 1 H, J = 3.1 Hz), 3.11 (dd, 1 H, J = 8.7, 15.2 Hz), 3.00 (m, 1 H), 2.89 (dd, 1 H, J = 8.2, 13.4 Hz), 2.80 (dd, 1 H, J = 6.9, 13.4 Hz), 2.25 (m, 1 H), 2.15 (m, 1 H), 1.79 (m, 1 H), 1.57−1.7 (m, 2 H), 1.56 (m, 3 H), 1.42 (m, 2 H), 0.87 (d, 3 H, J = 6.6 Hz), 0.81 (d, 3 H, J = 6.7 Hz). ^{13}C NMR (100 MHz, $CDCl_3$): δ 165.4, 162.9,148.8, 145.3, 137.7, 129.7, 129.5, 126.3, 125.7, 124.6, 123.2, 120.0, 114.3, 73.4, 58.6, 55.6, 53.9, 52.9, 30.5, 27.1, 26.9, 24.0, 22.3, 20.0, 19.9. MS-ESI (*m/z*): 547.2 (M + H)$^+$. HRMS-ESI (*m/z*) [M + Na]$^+$ calcd for $C_{28}H_{38}N_2O_7NaS$, 569.2299; found, 569.2297.

(2″*R*,14*S*)-*N*-[2″-Hydroxy-2″-(4-hydroxy-16-oxo-7,10,11,-12,13,14,15,16-octahydro-6*H*-5-oxa-15-aza-benzocyclotetradecen-14-yl)ethyl]-N-isobutyl-4-methoxy-benzenesulfonamide (23). To a stirring solution of 29 mg (0.046 mmol) of **20** in 25 mL of CH_2Cl_2 at 23 °C was added 3.6 mg (0.0044 mmol) of Grubbs' catalyst. The solution was stirred at 23 °C for 13.5 h and then concentrated. Purification by flash silica gel chromatography (35−40% EtOAc/hexanes) resulted in **23** (25 mg) as a white solid (89%) as a mixture of isomers (10:1). IR (neat): 3340, 1634, 1577, 1530, 1332 cm^{-1}. ^{1}H NMR of major isomer (500 MHz, $CDCl_3$): δ 7.69 (d, 2 H, J = 8.9 Hz), 7.51 (m, 2 H), 7.10 (m, 2 H), 6.94 (d, 2 H, J = 8.9 Hz), 5.78 (ddd, 1 H, J = 5.5, 10.9, 14.9 Hz), 5.50 (m, 1 H), 5.47 (s, 1 H), 4.16 (d, 1 H, J = 4.7 Hz), 3.99 (m, 2 H), 3.86 (s, 3 H), 3.81 (m, 1 H), 3.18 (dd, 1 H, J = 2.8, 15.1 Hz), 3.07 (dd, 1 H, J = 8.4, 15.1 Hz), 2.91 (d, 2 H, J = 7.6 Hz), 2.59 (m, 1 H), 2.44 (m, 1 H), 2.19 (m, 2 H), 1.85 (m, 1 H), 1.74 (m, 1 H), 1.65−1.42 (m, 5 H), 1.36 (m, 1 H), 0.86 (d, 3 H, J = 6.6 Hz), 0.84 (d, 3 H, J = 6.7 Hz). ^{13}C NMR (125 MHz, $CDCl_3$): δ 166.8, 163.3, 149.4, 144.8, 133.2, 130.8, 129.8, 128.5, 127.2, 125.6, 123.3, 120.0, 114.7, 75.9, 74.4, 58.4, 56.0, 55.1, 53.4, 34.2, 29.5, 27.3, 26.8, 25.3, 22.7, 20.5, 20.4.

(2″*R*,15*S*)-*N*-[2″-Hydroxy-2″-(4-hydroxy-17-oxo-6,7,8,-11,12,13,14,15,16,17-decahydro-5-oxa-16-aza-benzocyclopentadecen-15-yl)ethyl]isobutyl-4-methoxy-benzenesulfonamide (24). Acyclic diene **21** was subjected to the conditions of olefin metathesis as described for **20** resulting in **24** (29 mg, 89%) as a white solid (2:1 mixture). IR (neat): 3338, 1640, 1596, 1530 cm^{-1}. ^{1}H NMR of major isomer (400 MHz, $CDCl_3$): δ 7.71 (d, 2 H, J = 8.9 Hz), 7.37 (m, 1 H), 7.06 (m, 2 H), 6.95 (d, 2 H J = 8.8 Hz), 5.78 (s, 1 H), 5.42 (m, 1 H), 5.25 (m, 1 H), 4.11 (m, 1H), 4.04 (m, 1 H), 3.86 (m, 4 H), 2.9 (d, 1 H, J = 2.9 Hz), 3.2 (dd, 1 H, J = 9.0, 15.2 Hz), 2.97 (m, 2 H), 2.81 (dd, 1 H, J = 6.8, 15.0 Hz), 2.30−2.00 (m, 3 H), 2.00−1.80 (m, 3 H), 1.70 (m, 1 H), 1.57 (m, 4 H), 1.4 (m, 2 H), 1.3 (m, 2 H), 0.91 (d, 3 H, J = 6.7 Hz), 0.85 (d, 3 H, J = 6.7 Hz). ^{13}C NMR (100 MHz, $CDCl_3$): δ 165.6, 163.0, 149.1, 144.4, 131.6, 130.5, 129.5, 126.6, 124.8, 121.8, 118.5, 114.4, 75.4, 74.4, 73.2, 58.7, 55.6, 53.9, 52.7, 30.9, 29.0, 27.6, 27.5, 27.2, 26.7, 24.0, 20.1, 19.9.

(1′*S*,1″*R*)-2,3-Dihydroxy-N-(1′-{1″-hydroxy-2″-[isobutyl-(4-methoxy-benzenesulfonyl)amino]ethyl}octyl)-benzamide (25). To a stirred solution of **22** (20.4 mg, 0.03 mmol), 2.8 mg of 10% Pd−C in 6 mL of MeOH was added, and the resulting suspension was stirred at 23 °C under H_2 balloon for 3 h. The mixture was filtered through Celite and concentrated. Flash silica gel chromatography (35% EtOAc/ hexanes) provided **25** (12.9 mg, 63%); mp 44−46 °C; $[\alpha]_D^{23}$ +3.6 (*c* 0.30, $CHCl_3$). IR (neat): 3381, 2926, 1640, 1595, 1540, 1459, 1331, 1264, 1150, 1091, 1025, 806, 760 cm^{-1}. ^{1}H NMR (500 MHz, $CDCl_3$): δ 7.70 (dd, 1 H, J = 3.0, 11.9 Hz), 7.69 (dd, 1 H, J = 2.0, 6.9 Hz), 7.07 (d, 1 H, J = 7.2 Hz), 7.02 (dd, 1 H, J = 1.1, 8.2 Hz), 6.96 (dd, 1 H, J = 1.6, 5.6 Hz), 6.95 (dd, 1 H, J = 2.3, 11.8 Hz), 6.80 (m, 2 H), 5.80 (s, 1 H), 4.14 (qd, 1 H, J = 4.3, 13.7 Hz), 3.94 (td, 1 H, J = 4.1, 11.6 Hz), 3.86 (s, 3 H), 3.54 (d, 1 H, J = 3.7 Hz), 3.09 (m, 2 H), 2.92 (dd, 1 H, J = 7.8, 13.4 Hz), 2.87 (dd, 1 H, J = 7.3, 13.4 Hz), 1.86 (septet, 1 H, J = 6.8 Hz), 1.69 (m, 2 H), 1.25−1.30 (m, 9 H), 0.90 (d, 3 H, J = 6.3 Hz), 0.89 (d, 3 H, J = 6.3 Hz), 0.86 (t, 3 H, J = 6.9 Hz). ^{13}C NMR (125 MHz, $CDCl_3$): δ 170.6, 163.5, 149.6, 146.3, 130.0, 129.9, 119.2, 118.7, 116.6, 114.8, 114.1, 73.5, 59.3, 56.0, 53.9, 53.3, 32.2, 29.8, 29.7, 29.6, 27.7, 26.6, 23.0, 20.5, 20.4, 14.5. MS-ESI (*m/z*): 573.3 (M + Na)$^+$. HRMS-ESI (*m/z*) [M + Na]$^+$ calcd for $C_{28}H_{42}N_2O_7NaS$, 573.2613; found, 573.2610.

(2″*R*,14*S*)-*N*-[2″-Hydroxy-2″-(4-hydroxy-16-oxo-7,8,9,-10,11,12,13,14,15,16-decahydro-6*H*-5-oxa-15-aza-benzocyclotetradecen-14-yl)ethyl]-*N*-isobutyl-4-methoxy-benzenesulfonamide (26). A mixture of **23** (21 mg, 0.037 mmol) and 2.7 mg of 10% Pd−C in 10 mL of MeOH was stirred at 23 °C under H_2 balloon for 4 h. The mixture was then filtered through Celite and concentrated. Purification by flash silica gel chromatography (40% EtOAc/hexanes) provided **26** (14 mg, 69%) as a white solid; mp 63−65 °C. $[\alpha]_D^{23}$ +12.9 (*c* 0.35, $CHCl_3$). IR (neat): 3350, 1637, 1596, 1531, 1331 cm^{-1}. ^{1}H NMR (500 MHz, $CDCl_3$): δ 7.69 (dd, 1 H, J = 2.9, 11.7 Hz), 7.68 (dd, 1 H, J = 1.8, 7.0 Hz), 7.38 (dd, 1 H, J = 3.6, 5.9 Hz), 7.28 (d, 1 H, J = 7.3 Hz), 7.09 (m, 2 H), 6.94 (dd, 2 H, J = 2.9, 11.7 Hz), 5.79 (m, 1 H), 4.16−4.10 (m, 2 H), 3.86 (m, 4 H), 3.72 (d, 1 H, J = 3.2 Hz), 3.14 (dd, 1 H, J = 8.7, 15.2 Hz), 3.04 (dd, 1 H, J = 3.0, 15.2 Hz), 2.91 (dd, 1 H, J = 8.1, 13.4 Hz), 2.83 (dd, 1 H, J = 7.0, 13.4 Hz), 1.92 (m, 2 H), 1.82 (septet, 1 H, J = 6.9 Hz), 1.68 (m, 2 H), 1.57−1.37 (m, 9 H), 1.25 (m, 2 H), 0.87 (d, 3 H, J = 7.1 Hz), 0.83 (d, 3 H, J = 6.6 Hz). ^{13}C NMR (125 MHz, $CDCl_3$): δ 166.7, 163.4, 149.6, 144.5, 130.3, 129.9, 128.1,

125.5, 122.6, 119.4, 114.7, 75.6, 74.1, 59.0, 56.0, 54.0, 53.2, 28.5, 28.3, 27.5, 26.7, 24.4, 24.2, 23.6, 23.2, 20.5, 20.3. HRMS-ESI (*m/z*) [M + Na]$^+$ calcd for $C_{30}H_{44}N_2O_7NaS$, 599.2767; found, 599.2792.

(2″*R*,15*S*)-*N*-[2″-Hydroxy-2″-(4-hydroxy-17-oxo-6,7,8,9,-10,11,12,13,14,15,16,17-dodecahydro-5-oxa-16-aza-benzocyclopentadecen-15-yl)ethyl]-*N*-isobutyl-4-methoxy-benzenesulfonamide (27). Hydrogenation of **24** following the procedure for **26** resulted in **27** (13 mg, 78%) as a white solid; mp 69−72.5 °C. $[\alpha]_D^{23}$ +9.3 (*c* 0.49, $CHCl_3$). IR (neat): 3343, 1638, 1596, 1577, 1531, 1332 cm^{-1}. ^{1}H NMR (500 MHz, $CDCl_3$): δ 7.69 (m, 2 H), 7.28 (d, 1 H, *J* = 2.2 Hz), 7.18 (dd, 1 H, *J* = 8.9 Hz), 7.06 (m, 2 H), 6.94 (d, 2 H, *J* = 8.9 Hz), 5.90 (s, 1 H), 4.13 (m, 2 H), 3.96−3.87 (m, 2 H), 3.85 (s, 3 H), 3.84 (d, 1 H, *J* = 3.3 Hz), 3.12 (dd, 1 H, *J* = 8.4, 15.2 Hz), 3.05 (dd, 1 H, *J* = 3.1, 15.2 Hz), 2.92 (dd, 1 H, *J* = 8.1, 13.4 Hz), 2.86 (dd, 1 H, *J* = 7.0, 13.3 Hz), 1.90 (m, 2 H), 1.84 (m, 1 H), 1.73−1.66 (m, 3 H), 1.50−1.36 (m, 11 H), 0.89 (d, 3 H, *J* = 6.6 Hz), 0.85 (d, 3 H, *J* = 6.6 Hz). ^{13}C NMR (125 MHz, $CDCl_3$): δ 167.1, 163.4, 149.7, 144.4, 130.3, 129.9, 128.6, 125.2, 121.8, 119.0, 114.7, 75.1, 73.7, 59.1, 56.0, 54.1, 53.1, 29.4, 28.1, 27.6, 26.6, 26.0, 25.3, 24.6, 24.1, 23.5, 20.5, 20.3. MS-ESI (*m/z*): 599.3 [M + Na]$^+$. HRMS-ESI (*m/z*) [M + Na]$^+$ calcd for $C_{30}H_{44}N_2O_7$-NaS, 599.2769; found, 599.2767.

(1″*S*,1‴*R*)-2-But-3′-enyloxy-3-hydroxy-*N*-(1″-{1‴-hydroxy-2‴-[isobutyl-(4-methoxy-benzenesulfonyl)amino]-ethyl}hex-5″-enyl)benzamide (29). Acid **10** was coupled with amine **28** according to the general procedure for **19** to give **29** in 45% yield as an oil: $[\alpha]_D^{23}$ −4.4 (*c* 3.1, $CHCl_3$). IR (neat): 3344, 2958, 1632, 1577, 1534, 1497, 1462, 1333, 1260, 1152, 1091, 1023, 995, 807, 757 cm^{-1}. ^{1}H NMR (400 MHz, $CDCl_3$): δ 7.72 (d, 2 H, *J* = 8.8 Hz), 7.48 (dd, 1 H, *J* = 2.2, 7.3 Hz), 7.10 (m, 2 H), 6.97 (d, 2 H, *J* = 8.8 Hz), 5.96 (tdd, 1 H, *J* = 6.9, 10.2, 17.2 Hz), 5.82 (s, 1 H), 5.77 (tdd, 1 H, *J* = 6.8, 10.2, 16.9 Hz), 5.31 (m, 1 H), 4.98 (m, 1 H), 4.09 (m, 2 H), 3.94 (m, 2 H), 3.87 (s, 3 H), 3.79 (d, 1 H, *J* = 3.1 Hz), 3.21 (dd, 1 H, *J* = 9.2, 15.2 Hz), 2.99 (m, 2 H), 2.82 (dd, 1 H, *J* = 6.6, 13.3 Hz), 2.57 (m, 2 H), 2.09 (m, 2 H), 1.86 (m, 1 H), 1.62−1.70 (m, 2 H), 1.52−1.58 (m, 2 H), 1.43−1.52 (m, 3 H), 0.92 (d, 3 H, *J* = 6.6 Hz), 0.86 (d, 3 H, *J* = 6.6 Hz). ^{13}C NMR (125 MHz, $CDCl_3$): δ 165.8, 163.5, 149.6, 144.3, 138.7, 134.6, 130.3, 129.9, 127.2, 125.8, 122.6, 119.7, 119.5, 115.4, 114.8, 74.8, 73.5, 59.1, 56.0, 54.1, 53.0, 34.6, 34.0, 28.7, 27.7, 25.8, 20.5, 20.3. MS-ESI (*m/z*): 597.2 [M + Na]$^+$.

(2″*R*,13*S*)-*N*-[2″-Hydroxy-2″-(4-hydroxy-15-oxo-6,7,8,9,-10,11,12,13,14,15-decahydro-5-oxa-14-aza-benzocyclotridecen-13-yl)ethyl]-*N*-isobutyl-4-methoxybenzenesulfonamide (30). Acyclic diene **29** (42 mg) was cyclized under the conditions of olefin metathesis as described for **19** to give the corresponding cyclic olefin (37.7 mg, 75%, 1.9:1 mixture) as as a foam. IR (neat): 3347, 2958, 1633, 1596, 1577, 1535, 1497, 1463, 1332, 1290, 1260, 1152, 1091, 1025, 998, 807, 755 cm^{-1}; major isomer. ^{1}H NMR (500 MHz, $CDCl_3$): δ 7.84 (d, 1 H, *J* = 6.9 Hz), 7.67 (d, 2 H, *J* = 8.9 Hz), 7.51 (dd, 1 H, *J* = 2.0, 7.6 Hz), 7.02 (m, 2 H), 6.91 (d, 2 H, *J* = 8.9 Hz), 6.52 (s, 1 H), 5.60 (dd, 1 H, *J* = 6.12, 15.7 Hz), 5.55 (dd, 1 H, *J* = 5.5, 15.6 Hz), 4.26 (m, 2 H), 4.16 (m, 1 H), 3.95 (m, 1 H), 3.84 (s, 3 H), 3.15 (dd, 1 H, *J* = 3.2, 15.2 Hz), 3.00 (dd, 1 H, *J* = 8.4, 15.2 Hz), 2.90 (m, 2 H), 2.44 (m, 1 H), 2.35 (m, 1 H), 1.87 (m, 2 H), 1.81 (m, 1 H), 1.75 (m, 1 H), 1.67 (m, 2 H), 1.53 (m, 1 H), 0.83 (dd, 6 H, *J* = 6.7, 8.7 Hz). ^{13}C NMR (125 MHz, $CDCl_3$): δ 166.8, 163.3, 149.5, 144.6, 134.0, 130.5, 129.9, 128.4, 127.0, 124.6, 123.3, 120.5, 114.7, 74.1, 73.8, 58.7, 56.0, 54.1, 53.6, 32.4, 31.5, 27.6, 27.4, 24.4, 20.4, 20.4.

Hydrogenation of above olefin mixture for 1 h following the procedure for **26** resulted in saturated macrocycle **30** as a colorless solid (15.7 mg) in 71% yield; mp 74−75.5; $[\alpha]_D^{23}$ +29.9 (*c* 0.73, $CHCl_3$). IR (neat): 3348, 2951, 2931, 1635, 1596, 1577, 1534, 1497, 1464, 1332, 1288, 1260, 1151, 1091, 1025, 996, 807, 755 cm^{-1}. ^{1}H NMR (500 MHz, $CDCl_3$): δ 7.66 (d, 2 H, *J* = 8.9 Hz), 7.27 (m, 2 H), 7.04 (m, 2 H), 6.92 (d, 2 H, *J* = 8.9 Hz), 5.95 (s, 1 H), 4.12 (m, 2 H), 3.91 (m, 1 H), 3.85 (bs, 4 H), 3.08 (d, 2 H, *J* = 4.2, Hz), 2.86 (d, 2 H, *J* = 7.5 Hz), 1.93 (m, 1 H), 1.86 (m, 1 H), 1.79 (pentet, 1 H, *J* = 6.8 Hz), 1.69 (m, 4 H), 1.58 (m, 2 H), 1.48 (m, 3 H), 1.42 (m, 2 H), 0.86 (d, 3 H, *J* = 6.6 Hz), 0.82 (d, 3 H, *J* = 6.6 Hz). ^{13}C NMR (125 MHz, $CDCl_3$): δ 167.1, 163.4, 149.4, 144.4, 130.2, 129.9, 128.5, 125.1, 122.2, 119.3, 114.7, 74.1, 73.4, 59.0, 56.0, 54.2, 52.7, 29.5, 27.8, 27.5, 26.3, 24.1, 21.5, 21.4, 20.4, 20.3. HRMS-ESI (*m/z*) [M + K]$^+$calcd for $C_{29}H_{42}N_2O_7NaS$, 585.2610; found, 585.2591.

(1″*S*,1‴*R*)-N-(1″-[{2‴-Benzo[1⁗,3⁗]dioxole-5⁗-sulfonyl)isobutyl-amino]-1‴-hydroxyl-ethyl}hept-6″-enyl)-2-but-3′-enyloxy-3-hydroxy-benzamide (32). Acid **10** and amine **31** were coupled according to the method used for **19** to give **32** (38 mg, 57%) as a yellow oil: $[\alpha]_D^{23}$ −12.2 (*c* 0.18, $CHCl_3$). IR (neat): 3355, 1638, 1576, 1536, 1331 cm^{-1}. ^{1}H NMR (500 MHz, $CDCl_3$): δ 7.68 (d, 1 H, *J* = 8.6 Hz), 7.48 (dd, 1 H, *J* = 2.2, 7.3 Hz), 7.34 (dd, 1 H, *J* = 1.8, 6.4 Hz), 7.20 (d, 1 H, *J* = 1.8 Hz), 7.10 (m, 2 H), 6.88 (d, 1 H, *J* = 8.2 Hz), 6.09 (s, 2 H), 5.96 (tdd, 1 H, *J* = 6.9, 10.3, 17.1 Hz), 5.77 (m, 2 H), 5.33 (dd, 1 H, *J* = 1.4, 17.2 Hz), 5.29 (d, 1 H, *J* = 10.3 Hz), 4.98 (m, 1 H), 4.92 (d, 1 H, *J* = 10.2 Hz), 4.09 (m, 2 H), 3.97 (m, 2 H), 3.79 (d, 1 H, *J* = 3.29 Hz), 3.79 (d, 1 H, *J* = 3.3 Hz), 3.21 (dd, 1 H, *J* = 9.0, 15.1 Hz), 3.04 (d, 1 H, *J* = 2.6 Hz), 3.00 (m, 1 H), 2.85 (dd, 1 H, *J* = 6.7, 13.4 Hz), 2.57 (m, 2 H), 2.04 (dd, 2 H, *J* = 6.8, 11.9 Hz), 1.87 (ddd, 1 H, *J* = 6.7, 6.7, 14.8 Hz), 1.64 (m, 2 H), 1.45 (m, 2 H), 1.39 (m, 1 H), 0.92 (d, 3 H, *J* = 6.6 Hz), 0.87 (d, 3 H, *J* = 6.6 Hz). ^{13}C NMR (100 MHz, $CDCl_3$): δ 165.5, 151.5, 149.2, 148.3, 143.9, 138.6, 134.1, 131.6, 126.8, 125.4, 123.1, 122.2, 119.3, 119.1, 114.6, 108.4, 107.5, 102.4, 74.4, 73.1, 58.7, 53.6, 52.9, 34.1, 33.6, 29.7, 28.8, 27.2, 25.7, 20.1, 19.8. MS-ESI (*m/z*): 625.2 [M + Na]$^+$. HRMS-ESI (*m/z*) [M + Na]$^+$ calcd for $C_{31}H_{42}N_2O_8NaS$, 625.2562; found, 625.2560.

(2′*R*,14*S*)-Benzo[1″,3″]dioxole-5″-sulfonic Acid [2′-Hydroxy-2′-(4-hydroxy-16-oxo-7,8,9,10,11,12,13,14,15,16-decahydro-6*H*-5-oxa-15-aza-benzocyclotetradecen-14-yl)ethyl]isobutyl-amide (33). Acyclic diene **32** (31 mg) was subjected to the conditions of olefin metathesis as described for **22** to provide the corresponding cyclic olefin (29 mg, 9:1 mixture) in 95% yield. IR (neat): 3350, 1634, 1576, 1530, 1330 cm^{-1}. ^{1}H NMR of major (trans) diastereomer (500 MHz, $CDCl_3$): δ 7.53 (m, 1 H), 7.31 (m, 1 H), 7.18 (m, 1 H), 7.11 (m, 2 H), 6.83 (d, 1 H, *J* = 8.2 Hz), 6.08 (s, 2 H), 5.8 (m, 1 H), 5.5 (m, 2 H), 4.22 (d, 1 H, *J* = 4.9 Hz), 3.98 (m, 3 H), 3.9 (m, 1 H), 3.21 (m, 1 H), 3.07 (dd, 1 H, *J* = 8.5, 15.2 Hz), 2.93 (m, 2 H), 2.60 (m, 1 H), 2.50 0.85 (d, 3 H, *J* = 6.8 Hz). ^{13}C NMR (125 MHz, $CDCl_3$): δ 166.8, 151.7, 149.4, 148.6, 144.8, 133.1, 132.6, 129.8, 128.5, 127.1, 125.6, 123.4, 123.3, 120.1, 108.7, 108.0, 102.7, 74.4, 58.4, 55.3, 53.3, 34.2, 29.5, 27.3, 26.9, 25.3, 22.7, 20.5, 20.3.

Hydrogenation of above olefin mixture according to the procedure for **26** afforded **33** (20 mg, 91%) as a white solid; mp 64−65.5 °C; $[\alpha]_D^{23}$ +15.5 (*c* 0.62, $CHCl_3$). IR (neat): 3348, 1637, 1532, 1329 cm^{-1}. ^{1}H NMR (500 MHz, $CDCl_3$): δ 7.38 (dd, 1 H, *J* = 3.1, 6.5 Hz), 7.31 (m, 2 H), 7.17 (d, 1 H, *J* = 1.7 Hz), 7.07 (m, 2 H), 6.83 (d, 1 H, *J* = 8.2 Hz), 6.07 (s, 2 H), 5.91 (s, 1 H), 4.20−4.04 (m, 2 H), 3.90−3.80 (m, 2 H), 3.76 (d, 1 H, *J* = 3.1 Hz), 3.16−3.07 (m, 2 H), 2.92 (dd, 1 H, *J* = 5.3, 13.4 Hz), 2.85 (dd, 1 H, *J* = 7.0, 13.4 Hz), 1.91 (m, 1H), 1.80 (m, 1 H), 1.69 (m, 3 H), 1.51−1.41 (m, 8 H), 1.26 (m, 2 H), 0.88 (d, 3 H, *J* = 6.7 Hz), 2.3 (m, 2 H), 1.87 (m, 1 H), 1.73 (m, 1 H),1.5 (m, 5 H), 0.87 (d, 3 H, *J* = 6.7 Hz), 6.6), 0.83 (d, 3 H, *J* = 6.6 Hz). ^{13}C (125 MHz, $CDCl_3$): δ 166.8, 151.9, 149.7, 148.7, 144.5, 132.0, 128.0, 125.5, 123.5, 122.6, 119.5, 108.8, 107.9, 102.7, 75.5, 74.1, 59.0, 54.0, 53.3, 28.5, 28.3, 27.5, 26.6, 24.4, 24.2, 23.5, 23.2, 20.5, 20.3. HRMS-ESI (*m/z*) [M + Na]$^+$ calcd for $C_{29}H_{40}N_2O_8SNa$, 599.2403; found, 599.2378.

Antiviral Assay. The activity of designated compounds against HIV-1LAI was determined as previously described.[3a] Briefly, MT-2 cells (2 × 10^3/well) were exposed to 100 50% tissue culture infectious doses (TCID50s) of HIV-1LAI in the presence of various concentrations of an agent, examined in 96 well microculture plates, and incubated at 37 °C for 7 days (final volume: 200 μL/well). After the medium was removed from each well, 10 μL of 3-(4,5-dimethylthiazol-2-yl)-2,5-diphenyltetrazolium bromide (MTT) solution (7.5 mg/mL) in phosphatate-buffered saline was added to each well in the

plate, followed by incubation at 37 °C for 2 h. After incubation, to dissolve the formazan crystals, 100 μL of acidified 2-propanol containing 4% (v/v) Triton X-100 was added to each well and the optical density (570 nm) was measured in a microplate reader (Vmax; Molecular Devices, Sunnyvale, CA). All assays were conducted in duplicate.

Acknowledgment. Financial support of this work by the National Institutes of Health (Grant GM 53386 to A.K.G.) and a grant for the promotion of AIDS research from the Ministry of Health, Labor and Welfare (Kosei-Rodosho) of Japan (to H.M.) is gratefully acknowledged.

Supporting Information Available: HRMS and HPLC data for compounds **19**–**22**, **25**–**27**, **30**, **32**, and **33**. This material is available free of charge via the Internet at http://pubs.acs.org.

References

(1) (a) Sepkowitz, K. A. AIDS—The first 20 years. *N. Engl. J. Med.* **2001**, *344*, 1764–1772. (b) Cihlar, T.; Bischofberger, N. Recent developments in antiretroviral therapies. *Ann. Rep. Med. Chem.* **2000**, *35*, 177–89. (c) Flexner, C. W. Pharmacogy of drug interactions of HIV protease inhibitors. In *Protease Inhibitors in AIDS Therapy*; Ogden, R. C., Flexner, C. W., Eds.; Marcel Dekker: New York, 2001; pp 139–160.

(2) (a) Ghosh, A. K.; Shin, D. W.; Swanson, L.; Krishnan, K.; Cho, H.; Hussain, K. A.; Walters, D. E.; Holland, L.; Buthod, J. Structure-based design of non-peptide HIV protease inhibitors. *Farmaco* **2001**, *56*, 29–32. (b) Ghosh, A. K.; Kincaid, J. F.; Cho, W.; Walters, D. E.; Krishnan, K.; Hussain, K. A.; Koo, Y.; Cho, H.; Rudall, C.; Holland, L.; Buthod, J. Potent HIV protease inhibitors incorporating high affinity P2-ligands and (*R*)-(hydroxyethylamino)sulfonamide isostere. *Bioorg. Med. Chem. Lett.* **1998**, *8*, 687–90.

(3) (a) Koh, Y.; Nakata, H.; Maeda, K.; Ogata, H.; Bilcer, G.; Devasamudram, T.; Kincaid, J. F.; Boross, P.; Wang, Y.-F.; Tie, Y.; Volarath, P.; Gaddis, L.; Harrison, R. W.; Weber, I. T.; Ghosh, A. K.; Mitsuya, H. A novel bis-tetrahydrofuranylurethane-containing non-peptide protease inhibitor (PI) UIC-94017 (TMC-114) potent against multi-PI-resistant HIV in vitro. *Antimicrob. Agents Chemother.* **2003**, *47*, 3123–29. (b) Yoshimura, K.; Kato, R.; Kavlick, M. F.; Nguyen, A.; Maroun, V.; Maeda, K.; Hussain, K. A.; Ghosh, A. K.; Gulnik, S. V.; Erickson, J. W.; Mitsuya, H. *UIC-94003*: A potent protease inhibitor (PI) that inhibits multi-PI-resistant HIV-1 peplication in vitro. *J. Virol.* **2002**, *76*, 1349–1358.

(4) (a) Ghosh, A. K.; Leshchenko, S.; Noetzel, M. Stereoselective photochemical 1,3-dioxalene addition to α,β-unsaturated-γ-lactone: Synthesis of bis-tetrahydrofuranyl ligand for HIV protease inhibitor UIC-94-017 (TMC-114). *J. Org. Chem.* **2004**, *69*, 7822–29. (b) Ghosh, A. K.; Chen, Y. Synthesis and optical resolution of high affinity P_2-ligands for HIV-1 protease inhibitors. *Tetrahedron Lett.* **1995**, *36*, 505. (c) Ghosh, A. K.; Kincaid, J. F.; Walters, D. E.; Chen, Y.; Chaudhuri, N. C.; Thompson, W. J.; Culberson, C.; Fitzgerald, P. M. D.; Lee, H. Y.; McKee, S. P.; Munson, P. M.; Duong, T. T.; Darke, P. L.; Zugay, J. A.; Schleif, W. A.; Axel, M. G.; Lin, J.; Huff, J. R. Nonpeptidal P_2-ligands for HIV protease inhibitors: Structure-based design, synthesis and biological evaluation. *J. Med. Chem.* **1996**, *39*, 3278–90.

(5) Tie, Y.; Boross, P. I.; Wang, Y.-F.; Gaddis, L.; Hussain, A. K.; Leshchenko, S.; Ghosh, A. K.; Louis, J. M.; Harrison, R. W.; Weber, I. T. High-resolution crystal structures of HIV-1 protease with a potent non-peptide inhibitor (UIC-94017) active against multi-drug resistant clinical strains. *J. Mol. Biol.* **2004**, *338*, 341–352.

(6) De Meyers, S.; Peeters, M. Conference on Retroviruses and Opportunistic Infections (11th CROI), February 8–11, 2004, San Francisco, CA; Abstracts 533 and 620.

(7) (a) Mitsunobu, O. The use of diethyl azodicarboxylate and triphenylphosphine in synthesis and transformation of natural products. *Synthesis* **1981**, 1–28.

(8) Gao, Y.; Hanson, R. M.; Klunder, J. M.; Ko, S. Y.; Masamune, H.; Sharpless, K. B. Catalytic asymmetric epoxidation and kinetic resolution: Modified procedures including in situ derivatization. *J. Am. Chem. Soc.* **1987**, *109*, 5765–5780.

(9) Caron, M.; Carlier, P. R.; Sharpless, K. B. Regioselective azide opening of 2,3-epoxy alcohols by $[Ti(O\text{-}i\text{-}Pr)_2(N_3)_2]$: Synthesis of α-amino acids. *J. Org. Chem.* **1988**, *53*, 5185–5187.

(10) Ghosh, A. K.; McKee, S. P.; Lee, H. Y.; Thompson, W. J. A facile and enantiospecific synthesis of 2(S)- and 2(R)-[1′(S)-azido-2-phenylethyl] oxirane. *J. Chem. Soc. Chem. Commun.* **1992**, 273–274.

(11) Evans, B. E.; Rittle, K. E.; Homnick, C. F.; Springer, J. P.; Hirshfield, J.; Veber, D. F. A stereocontrolled synthesis of hydroxyethylene dipeptide isosteres using novel chiral, aminoalkyl epoxides and γ-(aminoalkyl) γ-lactones. *J. Org. Chem.* **1985**, *50*, 4615–4625.

(12) Grubbs, R. H.; Chang, S. Recent advances in olefin metathesis and its application in organic synthesis. *Tetrahedron* **1998**, *54*, 4413–4450.

(13) Bergmann, E.; Heimhold, H. Rearrangement of allyl ethers in the purine series, with some remarks on the hydrogenation of allyl ethers. *J. Chem. Soc.* **1935**, 1365–1367.

(14) Chung, S.-K. Selective reduction of mono- and disubstituted olefins by sodium borohydride and cobalt (II). *J. Org. Chem.* **1979**, *44*, 1014–1016.

(15) This arylsulfonyl chloride was prepared by bromination of 1,2-methylenedioxybenzene with NBS[16] and halogen–metal exchange with ^{n}BuLi in hexane at −78 °C followed by reaction of the lithium salt with SO_2Cl_2.

(16) Gensler, W. J.; Stouffer, J. E. Compounds related to podophyllotoxin. IX. 3,4-Methylenedioxyphenyllithium. *J. Org. Chem.* **1958**, *23*, 908.

(17) Toth, M. V.; Marshall, G. R. A simple, continuous fluorometric assay for HIV protease. *Int. J. Pept. Protein Res.* **1990**, *36*, 544–550.

(18) Roberts, N. A.; Martin, J. A.; Kinchington, D.; Broadhurst, A. V.; Craig, J. C.; Duncan, I. B.; Galpin, S. A.; Handa, B. K.; Kay, J.; Krohn, A.; Lambert, R. W.; Merrett, J. H.; Mills, J. S.; Parkes, K. E. B.; Redshaw, S.; Ritchie, A. J.; Taylor, D. L.; Thomas, G. J.; Machin, P. J. Rational design of peptide-based HIV proteinase inhibitors. *Science* **1990**, *248*, 358–361.

(19) (a) Noble, S.; Goa, K. L. Amprenavir: A review of its clinical potential in patients with HIV infection. *Drugs* **2000**, *60*, 1383–1410. (b) Kim, E. E.; Baker, C. T.; Dwyer, M. D.; Murcko, M. A.; Rao, B. G.; Tung, R. D.; Navia, M. A. Crystal structure of HIV-1 protease in complex with VX-478, a potent and orally bioavailable inhibitor of the enzyme. *J. Am. Chem. Soc.* **1995**, *117*, 1181–1182.

(20) Weiner, S. J.; Kollman, P. A.; Nguyen, D. T.; Case, D. A. An all atom force field for simulations of proteins and nucleic acids. *J. Comput. Chem.* **1986**, *7*, 230–252.

(21) To analyze the protein–ligand interactions of this class of inhibitors, crystallographic studies of the HIV-1 protease complex of inhibitor **26** are being attempted.

JM050019I

ELSEVIER

Neurobiology of Disease

www.elsevier.com/locate/ynbdi
Neurobiology of Disease 20 (2005) 12–26

Increase of C1q biosynthesis in brain microglia and macrophages during lentivirus infection in the rhesus macaque is sensitive to antiretroviral treatment with 6-chloro-2′,3′-dideoxyguanosine

Candan Depboylu,[a,b] Martin K.-H. Schäfer,[a] Wilhelm J. Schwaeble,[a,c] Todd A. Reinhart,[d] Hitomi Maeda,[e] Hiroaki Mitsuya,[e] Ruslan Damadzic,[f] Dianne M. Rausch,[g] Lee E. Eiden,[f] and Eberhard Weihe[a,*]

[a]*Department of Molecular Neuroscience, Institute of Anatomy and Cell Biology, Philipps University, Robert-Koch-Str. 8, 35033 Marburg, Germany*
[b]*Department of Neurology, Center for Nervous Diseases, Philipps University, Marburg, Germany*
[c]*Department of Infection, Immunity and Inflammation, University of Leicester, Leicester, UK*
[d]*Department of Infectious Diseases and Microbiology, University of Pittsburgh, Pittsburgh, PA 15260, USA*
[e]*Division of Cancer Treatment, National Cancer Institute, NIH, Bethesda, MD 20892, USA*
[f]*Section on Molecular Neuroscience, Laboratory of Cellular and Molecular Regulation, National Institute of Mental Health, NIH, Bethesda, MD 20892, USA*
[g]*Division of Mental Disorders, Behavioral Research and AIDS, National Institute of Mental Health, NIH, Bethesda, MD 20892, USA*

Received 5 November 2004; revised 26 January 2005; accepted 31 January 2005
Available online 22 March 2005

Complement activation in the brain contributes to the pathology of neuroinflammatory and neurodegenerative diseases such as neuro-AIDS. Using semiquantitative in situ hybridization and immunohistochemistry, we observed an early and sustained increase in the expression of C1q, the initial recognition subcomponent of the classical complement cascade, in the CNS during simian immunodeficiency virus (SIV) infection of rhesus macaques. Cells of the microglial/macrophage lineage were the sources for C1q protein and transcripts. C1q expression was observed in proliferating and infiltrating cells in SIV-encephalitic brains. All SIV-positive cells were also C1q-positive. Treatment with the CNS-permeant antiretroviral agent 6-chloro-2′,3′-dideoxyguanosine decreased C1q synthesis along with SIV burden and focal inflammatory reactions in the brains of AIDS-symptomatic monkeys. Thus, activation of the classical complement arm of innate immunity is an early event in neuro-AIDS and a possible target for intervention.

Keywords: Complement; Microglia; Neuro-AIDS; Antiretroviral treatment; Blood–brain barrier; Cell proliferation

Introduction

The complement system is a major component of the innate immune system. It is composed of more than thirty soluble and membrane-anchored proteins. Three possible complement activation cascades generate opsonins, inflammatory mediators, and cytolytic protein complexes which play an important role in clearing microorganisms and tissue damage products (Whaley and Schwaeble, 1997). Locally synthesized complement components and regulators are present at higher than normal levels in a variety of human and animal neurodegenerative (Farkas et al., 2003; Kovacs et al., 2004; Rostagno et al., 2002; Schäfer et al., 2000; Singhrao et al., 1996; Velazquez et al., 1997; Yamada et al., 1994) and neuroinflammatory diseases (Dietzschold et al., 1995; Walsh and Murray, 1998; Williams et al., 1994). Mice which are deficient in classical complement activation are partly protected against spongiform encephalopathy after intraperitoneal exposure to prion (Klein et al., 2001). On the other hand, complement activation can reduce neurodegeneration and plaque formation in a mouse model of Alzheimer's disease (Wyss-Coray et al., 2002).

Activation of complement was shown during the course of human immunodeficiency virus (HIV) infection in non-CNS tissues but little is known about the involvement of complement activation during HIV infection in the brain (Perricone et al., 1987; Senaldi et al., 1990). In vitro, complement activation may significantly enhance the infection of complement receptor-bearing cells by HIV-1 (Robinson et al., 1988, 1989, 1990; Sölder et al., 1989; Tremblay et al., 1990) or simian immunodeficiency virus (SIV) (Montefiori et al., 1990). Activation of the classical complement pathway in immunodeficiency virus infection may be through direct binding of C1q, the recognition subunit of the first complement component, to the retroviral glycoproteins

* Corresponding author. Fax: +49 6421 2868965.
E-mail address: weihe@staff.uni-marburg.de (E. Weihe).
Available online on ScienceDirect (www.sciencedirect.com).

0969-9961/$ - see front matter © 2005 Elsevier Inc. All rights reserved.
doi:10.1016/j.nbd.2005.01.030

gp41 or *gp120* (Ebenbichler et al., 1991), or as a result of interaction of C1q with immune complexes of envelope-specific antibodies.

The aims of this study were to investigate whether C1q is produced locally in the brain in the course of lentiviral infection, to identify the cell types responsible for the biosynthesis of C1q peptide chains, and to characterize the regulation of C1q expression through the disease process and therapeutic intervention. We used a well-established primate model for human HIV infection–SIV infection of rhesus macaques. Like HIV-infected individuals, rhesus monkeys infected with SIV develop acquired immunodeficiency syndrome (AIDS) and neurological complications including cognitive and motor deficits (Murray et al., 1992). Impairments occur with low or marked encephalitis with the appearance of astrogliosis, nodule and giant cell formation, inflammatory infiltrates, myelin pallor, and vessel leakage (Budka, 1986; Lane et al., 1996; Luabeya et al., 2000; Weihe et al., 1993). Loss of synapses, dendrites, and neurons also occurs in SIV disease (Bissel et al., 2002; Li et al., 1999; Luthert et al., 1995). Neurodegenerative damage is thought to be related to SIV replication, the number of inflammatory cells infiltrating and activated in the brain, and the amount of host- and/or virus-derived cytotoxins produced (Bissel et al., 2002; Glass et al., 1995; Li et al., 1999; Lipton et al., 1991; Power et al., 2002).

In order to understand the effect of CNS-permeant antiretroviral treatment on neurochemical sequelae during simian AIDS, we explored additionally the effects of the lipophilic antiretroviral agent 6-chloro-2′,3′-dideoxyguanosine (6-Cl-ddG) on C1q expression. 6-Cl-ddG is a congener of 2′,3′-dideoxyguanosine and penetrates efficiently into the CNS in monkeys (Hawkins et al., 1995). It is highly active against HIV-1 and SIV in vitro (Fujii et al., 1998; Shirasaka et al., 1990), and in vivo (Depboylu et al., 2004; Fujii et al., 1997a,b, 1998). Our data demonstrate a relationship between C1q expression and virus burden, as well as disease progression and CNS-directed antiretroviral therapy during lentiviral infection of the brain.

Materials and methods

Virus stock, inoculation procedures in rhesus monkeys, and antiretroviral treatment

Juvenile rhesus macaques, which were determined negative for simian retrovirus-1 and -2, simian immunodeficiency virus, and simian herpes virus, were inoculated intravenously with ten rhesus infectious doses of cell-free SIV_{6B670} grown in human peripheral blood mononuclear cells. Virus was obtained as an aliquot of a previously characterized virus stock stored in liquid nitrogen (da Cunha et al., 1995). Following inoculation, animals were monitored and examined for clinical evidence of disease. Blood and cerebrospinal fluid (CSF) samples were obtained from the animals at regular intervals. Eight macaques exhibited clinical signs of acquired immunodeficiency syndrome (AIDS) and five did not at time of euthanasia (Depboylu et al., 2004). AIDS-defining criteria included one or more of the following: more than 10% loss of body weight, intractable diarrhea/dehydration requiring fluid replacement, oral lesions, and organ inflammations. Additionally, four SIV-infected monkeys, in which the viral load was found to be more than 100,000 virions/mL in plasma and more than 100 virions/mL in CSF in more than two consecutive examinations, underwent a treatment with 2′,3′-dideoxyinosine (ddI) or 6-chloro-2′,3′-dideoxyguanosine (6-Cl-ddG), and were euthanized shortly thereafter (see Depboylu et al., 2004). Three monkeys (MO76, MO77, and MO91) received 10 mg/kg/day ddI subcutaneously for 3 weeks for clinical stabilization and then 75 mg/kg/day of 6-Cl-ddG subcutanously for 6 weeks. A fourth monkey (MO89) received only 6-Cl-ddG (200 mg/kg/day) subcutaneously for 3 weeks. The vehicle for ddI administration was phosphate-buffered saline (PBS), and for 6-Cl-ddG administration, the vehicle was 70% propylene glycol/30% PBS. Four age-matched non-infected macaques were used as controls. Experiments involving the use of rhesus macaques were approved by the Animal Care and Use Committee of Bioqual, Inc., an NIH-approved and Association for Assessment and Accreditation of Laboratory Animal Care-accredited research facility. All experiments were carried out using the ethical guidelines promulgated in the National Institutes of Health Guide for the Care and Use of Laboratory Animals.

Tissue preparation for histochemical analysis

Prior to sacrifice, animals received ketamine (20 mg/kg) and were then anesthetized sequentially with ketamine–acepromazine (10 mg/kg) and perfused transcardially in the following sequence: 2 L/kg PBS, then 400 mL/kg of 1% formalin in PBS, followed by 1.5 L/kg of 4% formalin in PBS. Tissue specimens were obtained at necropsy and immersion-fixed overnight in 4% paraformaldehyde/PBS. Next, some blocks were cryopreserved in 10–20% sucrose in PBS and snap frozen in isopentane cooled to −70°C. Some blocks were postfixed in Bouin–Hollande solution (containing 4% picric acid, 2.5% cupric acetate, 3.7% formaldehyde, and 1% glacial acetic acid) or buffered formalin, followed by extensive washes in 70% 2-propanol, dehydration, and processing for paraffin embedding.

Generation of specific complementary RNA probes

Specific sense and antisense riboprobes were generated from linearized vector constructs by in vitro transcription using the appropriate RNA polymerases and [^{35}S]-UTP and digoxigenin-UTP as label. Vectors with inserts were pBluescript KS+ containing an ~0.65-kb fragment of human C1q A cDNA, pBluescript KS+ containing an ~0.4-kb fragment of human C1q B cDNA and pGEM-T easy containing an ~0.45-kb fragment of human C1q C cDNA, respectively (Sellar et al., 1991). To increase tissue penetration of probes, the generated cRNA transcripts were reduced to nucleotide fragments of approximately 200–250 nucleotides by limited alkaline hydrolysis. The specificity of in situ hybridization signals was assessed by performing experiments with cRNA probes in sense strand orientation on subjacent sections.

Radioactive and non-radioactive in situ hybridization (ISH) histochemistry

ISH was performed according to the protocol reported by Schäfer et al. (1992) with some modifications (Depboylu et al., 2004). Frozen sections (14 μm) were cut from cryopreserved tissues, and thaw-mounted on superfrost plus microscope slides. Alternatively, paraffin embedded formalin-fixed brain tissue

sections (10 μm) were cut, deparaffinized in xylene, and rehydrated through graded series of 2-propanol. For pretreatment, sections were boiled in 10 mM sodium citrate buffer (pH 6.0) at 95°C for 15 min, washed in 10 mM PBS and in 0.4% Triton X-100/PBS. After rinsing in distilled water, sections were acetylated with triethanolamine/acetic anhydride (pH 8.0) for 10 min at room temperature (RT), followed by a wash in distilled water, and then dehydrated in graded ethanols, air dried, and directly used for hybridization, or stored at −20°C until use.

For radioactive hybridization, sections were incubated with cRNA probes diluted in hybridization buffer {50% formamide, 10% dextran sulfate, 3× saline sodium citrate (SSC), 50 mM sodium phosphate (pH 7.4), 10 mM dithiothreitol (DTT), 1× Denhardt's solution [0.02% Ficoll 400, 0.02% polyvinylpyrrolidone, 0.02% bovine serum albumine (BSA)], 0.1 mg/mL yeast tRNA} to a final concentration of 50×10^3 dpm/μL. DTT was added to a final concentration of 10 mM. 20- to 30-μL hybridization mix was applied and slides were coverslipped. Hybridization was carried out at 60°C in a humid chamber. After 16 h, coverslips were removed in 2× SSC at RT and the sections washed in the following order: 20 min in 1× SSC, 30 min RNAse buffer (10 mM Tris, pH 8.0, 0.5 M NaCl and 1.0 mM EDTA; containing 20 μg/mL RNAse A and 1 U/mL RNAse T1) at 37°C, in 1×, in 0.5×, and in 0.2× SSC each for 20 min, 60 min in 0.2× SSC at 60°C, and 10 min in 0.2× SSC and 5 min in distilled water at RT. The tissue was then dehydrated in graded ethanols and air dried. For visualization of hybridization signals, sections were coated with nitroblue tetrazolium (NBT)-2 nuclear emulsion (Eastman Kodak, Rochester, NY) and stored at 4°C. After 2–3 weeks of exposure, slides were developed (Kodak D19), fixed, counterstained with hematoxylin, dehydrated through graded series of ethanol, and coverslipped.

For non-radioactive detection, riboprobes were generated by in vitro transcription with a digoxigenin labeling mix containing 10 mM each of ATP, CTP, and GTP, 6.5 mM UTP, and 3.5 mM digoxigenin-11-UTP (Boehringer, Germany). After hydrolysis, probes were purified by sodium acetate precipitation and added in hybridization buffer to a final concentration of 1 ng/μL. Hybridization and washing procedures were performed as described above for radioactive detection. For the detection of non-radioactive hybrids, slides were equilibrated to buffer 1 (100 mM Tris and 150 mM sodium chloride, pH 7.5) containing 0.05% Tween 20 (Merck, Germany). Blocking was performed by incubation for 1 h in blocking buffer (buffer 1 containing 2% normal lamb serum). Alkaline phosphatase-conjugated anti-digoxigenin Fab fragments (Boehringer, Germany) were diluted to 1 U/mL in blocking buffer. After the slides were rinsed with buffer 1, the diluted antibody was applied for 1 h at RT. After washes in buffer 1, slides were equilibrated to buffer 2 (100 mM Tris, 100 mM sodium chloride, and 50 mM magnesium chloride, pH 9.4) containing 0.05% Tween 20 before a 72-h color reaction in buffer 2 containing 0.2 mM 5-bromo-4-chloro-3-indolyl phosphate (BCIP) and 0.2 mM NBT-2 salt (Boehringer, Germany) at 4°C. The reaction was stopped by washing the slides in distilled water, counterstained with hematoxylin, and coverslipped.

Hybridized sections were analyzed in dark or bright field illumination and photographed with the Olympus AX70 microscope (Olympus Optical, Germany).

Single enzymatic and single fluorescence immunohistochemistry (IHC)

A previously reported protocol for IHC was used with some modifications (Rohrenbeck et al., 1999; Schäfer et al., 2000). Deparaffinized paraffin-embedded tissue sections (7 μm) or cryosections (14 μm) were rehydrated through graded series of 2-propanol, incubated in methanol/H_2O_2 for 30 min, and boiled in 10 mM sodium citrate buffer (pH 6.0) at 95°C for 15 min. After several rinses in 50 mM PBS, sections were incubated in PBS containing 5% BSA for 30 min and in 1% BSA/PBS for 15 min. Thereafter sections were incubated with 30% avidin-blocking kit in 1% BSA/PBS and 30% biotin-blocking kit in 1% BSA/PBS (Vectastain Elite Avidin–Biotin-Blocking kit, Boehringer, Germany) for 15 min at RT. Then, primary antibodies were applied. A sheep polyclonal antibody against C1q protein (ICN Biochemicals, CA) which did not differentiate between the C1q A, B, and C chains was used at a 1:15,000 dilution. The proliferation marker Ki67 was detected with the mouse monoclonal antibody MIB-1 (Dianova, Germany) at a 1:200 dilution. Cells of mononuclear origin and endothelial cells were visualized with the biotinylated isolectin RCA-120 (Dianova, Germany) at a 1:5000 dilution. The primary antibodies were applied in 1% BSA/PBS and incubated at 16°C overnight followed by 2 h at 37°C and 2 h 27°C. After several washes in distilled water followed by rinsing in PBS, sections were incubated with species-specific biotinylated secondary antibodies (Dianova, Germany) for 1 h at 37°C, washed several times and incubated for 45 min with avidin–biotin–peroxidase complex reagents (Vectastain Elite ABC kit, Boehringer, Germany). Immunoreactions were visualized with 3,3′-diaminobenzidine (DAB, Sigma, Germany), resulting in a brown staining, or enhanced by the addition of 0.08% ammonium nickel sulfate (Fluka, Buchs, Switzerland), resulting in a dark blue staining. After three 5-min washes in distilled water, the sections were dehydrated through graded series of 2-propanol and coverslipped.

For immunofluorescence, C1q was detected with the sheep polyclonal antibody (ICN Biochemicals, CA) at a 1:1000 dilution. In addition, the following antibodies against brain resident cell markers were used. The mouse monoclonal antibody KP1 (DAKO, Denmark) recognized the macrophage activation marker molecule CD-68 and was used at a 1:50 dilution. Endothelial cells were visualized with a rabbit polyclonal antibody against von Willebrand factor (vWF; DAKO, Germany) at a 1:400 dilution. The biotinylated isolectin *ricinus communis* agglutinin-120 (RCA-120; Dianova, Germany) detected the cells of mononuclear origin and the endothelial cells (1:500 diluted). Neurons were visualized with a mouse monoclonal antibody recognizing the neuronal marker antigen NeuN (MAB377; Chemicon, Temecula, CA) at a 1:300 dilution. Astrocytes were stained with a polyclonal antibody from guinea pig against glial fibrillary acid protein (GFAP; 1:400 diluted; Progen, Germany). Oligodendrocytes were identified with a mouse monoclonal antibody Ab-1 recognizing 2′,3′-cyclic nucleotide-3′-phosphodiesterase (CNPase; Neomarkers, Fremont, USA) at a 1:50 dilution. Proliferating cells were visualized with the mouse monoclonal antibody MIB-1 against Ki67 (1:50 diluted). Immunoreactions were visualized by incubation with either species-specific indocarbocyamine-conjugated IgG (Cy3; Dianova, Germany), resulting in red–orange fluorescence labeling, or with species-specific biotinylated IgG (Dianova, Germany) both diluted 1:100 in 1% BSA/PBS for 1 h at 37°C and then, after a 15-min

wash in PBS, with Alexa 488-conjugated streptavidin (MoBiTec, Germany) at a 1:200 dilution in 1% BSA/PBS for 2 h at 37°C, resulting in green fluorescence. The biotinylated isolectin RCA-120 was visualized with Alexa 488-conjugated streptavidin. After extensive washes in distilled water, sections were further processed or coverslipped.

Fluorescence signals were analyzed and photographed with the Olympus AX70 microscope (Olympus Optical, Germany) or with the Olympus Fluoview confocal laser scanning microscope (Olympus Optical, Germany).

Double enzymatic and double fluorescence IHC

To visualize two different antigens in the same section, double IHC was carried out with primary antibodies from different species. The proliferation marker Ki67 was detected with nickel-enhanced DAB-visualization resulting in a nuclear dark blue staining. Prior to application of the antibody against C1q, the avidin–biotin–peroxidase from the first visualization procedure was blocked by incubation of sections in methanol/H_2O_2 and in avidin–biotin-blocking kit. C1q-immunoreactivity was visualized as described above but without nickel enhancement resulting in a cytoplasmic brown reaction product. To identify cell types immunopositive for C1q, double immunofluorescence for C1q and for the appropriate markers for brain resident cells (see above) was carried out. Sections were analyzed by high-power confocal laser scanning microscopy.

Double ISH histochemistry

Detection of two different RNA transcripts in the same tissue section was performed with radioactive and non-radioactive labeled riboprobes as described previously (Schäfer and Day, 1994). Digoxigenin-labeled and [^{35}S]-labeled probes were diluted in the same hybridization buffer in working concentrations. Hybridization and post-hybridization were carried out as described above. Non-radioactive signals were detected first. For the detection of radioactive-labeled probes, slides were air dried and covered with K5 photoemulsion (Ilford, England) diluted 1:1 in distilled water and stored at 4°C. Exposure times were 2–4 weeks.

Immunofluorescence combined with ISH histochemistry

For visualizing of an antigen with an RNA transcript in the same tissue section, IHC was performed in combination with ISH. Prehybridization, hybridization with the [^{35}S]-labeled probe against C1q A mRNA, and post-hybridization were performed. Before covering the slides with K5 photoemulsion (Ilford, England) for a 3-week exposure at 4°C, C1q or RCA-120 immunofluorescence staining was performed.

Detection of viral burden

Viral transcription and translation were detected by ISH and IHC. The monoclonal antibody KK41 against the SIV_{mac251} envelope glycoprotein *gp41* (NIH AIDS Research and Reference Program, Bethesda, MD, USA) was used to detect the crossreacting $SIV_{δB670}$ *gp41* (Kent et al., 1992). Single enzymatic (KK41 diluted 1:2000) and immunofluorescence (KK41 diluted 1:200) detection of *gp41* were carried out as described above. To assess the relationship of C1q with viral *gp41*, sections were co-stained for C1q and *gp41* double immunofluorescence as described above. ISH was performed using probes generated by incorporation of [^{35}S] into SIV RNA probes by in vitro transcription of SIV_{mac239} sequences cloned in a $pTRIK_{AN}19$ vector, or into DNA probes by random priming using sequences of cloned $SIV_{macBK28}$ DNA (Depboylu et al., 2004; Reinhart et al., 1997). Activities of radioactive probes were 30–50 × 10^3 dpm/μL. The DNA templates were a *Kpn*I fragment from the *pol* gene of SIV_{mac239} (nucleotide positions 5208–4713) or a *Bam*HI fragment from $SIV_{macBK28}$ (nucleotide positions 1841–9174). In some experiments, in situ hybridization experiments were performed with oligonucleotides specific for unspliced SIV RNA complementary to sequences at the exon/intron junction at the 5′-end of unspliced RNA (nucleotide positions 996–967 of SIV_{smH4} proviral sequence) as described by Reinhart et al. (1997). The sequences in the control sense probe were identical to sequences at the same exon/intron junction (nucleotide positions 967–996 of SIV_{smH4}). Polyacrylamide gel purified nucleotides were 3′-end-labeled with [^{35}S]-dCTP using terminal deoxynucleotide transferase to specific activities of 2–8 × 10^9 cpm/μg. For ISH, slide-mounted sections (14 μm) of cryopreserved tissues were postfixed in 4% paraformaldehyde/PBS, washed, and dehydrated. Pretreatments consisted of incubation for 20 min each in 0.2 N HCl at ambient temperature; 2× SSC at 70°C; and 2 mM $CaCl_2$, 20 mM Tris (pH 7.5), and 10 μg/mL proteinase K at 37°C, followed by washing, acetylation, and dehydration. Sections were then hybridized for 18 h at 45°C (for riboprobes) or at 37°C (for oligonucleotide probes). After post-hybridization, sections were coated with NTB-2 emulsion and exposed at 4°C for 3–6 days. After development, the sections were counterstained with cresyl violet.

Quantification of C1q A mRNA-positive cells

The average number of C1q A mRNA-positive cells was determined by cell counts in at least 15 random areas (each 0.1 mm^2) per section of striatum and insular cortex in a magnification which allowed the discrimination of cellular features. Three to eight interval sections of striatum and insular cortex were analyzed per animal. Cells with a nucleus were accepted as positive when having greater number of silver grains over their cytoplasm than background. Each multinucleated giant cell and cluster of cells, where the individual cell borders could not be distinguished, were counted as single cells. Quantitative image analysis was performed with the MCID M4 image analysis system (Imaging Research, St. Catharines, ON, Canada). Data were expressed as mean number (±SEM) of positive cells per 0.1 mm^2 area per experimental group.

Quantification of silver grains per C1q A mRNA-positive cell

After radioactive ISH, the number of silver grains per C1q A mRNA-positive cell in striatum and insular cortex were counted under highest magnification. Three to eight interval sections of striatum and insular cortex per monkey were analyzed. At least 20 random cells per section of striatum and insular cortex were analyzed by computer-assisted image analysis (MCID M4 image analysis system, Imaging Research, St. Catharines, ON, Canada). Multinucleated giant cells and clusters of cells, where the cell